Phase diagram and magnetic structures of CeSb

J. Rossat-Mignod, P. Burlet, and J. Villain
Laboratoire de Diffraction Neutronique Département de Recherche Fondamentale, Centre d'Etudes Nucléaires, 85-38041, Grenoble Cedex, France

H. Bartholin, Wang Tcheng-Si,* and D. Florence
Laboratoire de Magnétisme and Service National des Champs Intenses, Centre National de la Recherche Scientifique, 166X-38042, Grenoble Cedex, France

O. Vogt
Laboratorium für Festkörperphysik, Eidgenössische Technische Hochschule, Zürich, Switzerland
(Received 2 August 1976)

Among cerium pnictides, the compound CeSb exhibits the most complex behavior. The magnetic structures of the numerous observed phases have been determined. The magnetic field has been applied along a fourfold axis of the rock salt structure. For all the phases the order consists of square-wave structures characterized by a propagation vector $\vec{k} = (0,0,k)$ of value commensurate with the crystallographic cell and by a strong anisotropy confining the moments along the k vector. All the structures can be generated by a periodic stacking of zero magnetized planes P and ferromagnetic planes with a magnetization parallel $M\uparrow$ or antiparallel $M_\downarrow$ to the applied field. Three types of structures can be distinguished: (a) at low temperature only $M\uparrow$ and $M_\downarrow$ planes exist, the structures $k = 4/7$ $(++--++-)$, $k = 2/3$ $(++-)$, and $k = 0$ are successively observed when the field is increased. (b) at high temperature and low field $M\uparrow$, $M_\downarrow$, and P planes coexist leading to an "antiferroparamagnetic order." (c) at high temperature and high field only $M\uparrow$ and P planes exists defining a ferroparamagnetic order. The phase diagram feature can be understood by a simple thermodynamic analysis considering an entropy $S_0 = k\ln 2$ for paramagnetic planes and a moment of 2.1 μ_B/Ce atom for magnetized planes.

I. INTRODUCTION

During the last ten years a great amount of work has been done on cerium monopnictide compounds. In spite of their simple rocksalt crystallographic structure, all of them exhibit different magnetic behavior. Among these compounds the magnetic behavior of CeSb is the most complicated and is still not well understood. The purpose of this paper is to clarify this behavior, but in order to put our work in context we will first summarize briefly other studies which have been done on these compounds. Some results are reported in Table I.

In CeN,[1-3] cerium ions are predominantly tetravalent at room temperature and no magnetic ordering has been observed. CeP, CeAs, CeBi, and CeSb exhibit magnetic susceptibility anomalies at low temperatures.[4-6] CeBi and CeSb follow a Curie-Weiss law down to the ordering temperatures, 25 and 16 K, respectively. Below these temperatures, the thermal variation of the reciprocal susceptibility shows a minimum followed by a maximum.

CeAs and CeP susceptibilities follow a Curie-Weiss law only down to 120 K whereas their ordering temperatures are 7.5 and 9 K, respectively.[5] Below this temperature they exhibit a fcc type-I magnetic structure,[7,8] i.e., the propagation vector is $\vec{k} = (0, 0, 1)$ $(q = 2\pi k/a)$, with the moments oriented along the [001] direction [for CeAs $\mu = (0.68 \pm 0.07)\mu_B$].[7] The deviation from the Curie-Weiss law was first attributed to a continuous valence change ($Ce^{3+} \rightarrow Ce^{4+}$) of the cerium ions with decreasing temperature.[5] However, Jones,[9,10] Rainford *et al.*,[7] and Wang and Cooper[11] have shown that these susceptibility anomalies can be explained by crystal-field effects if the ground state is a Γ_7 doublet well isolated from the quadruplet state $\Gamma_8(\Delta = 140 \pm 10)$K for CeAs.[7] If the magnetic properties of CeAs and CeP seem well understood, this is not the case for CeBi and CeSb in the ordered state.

Below T_N, high-field magnetization measurements[5,6,12-17] have revealed a complex magnetic behavior for CeBi and CeSb; multiple-step magnetization processes with large hysteresis effects are observed with increasing and decreasing temperature. This behavior was also confirmed by magnetostriction measurements.[18] At low temperatures the main magnetization step value corresponds to one half the saturated value for CeBi and one third for CeSb. However, for CeSb, this magnetization step value becomes one half the saturated value at higher temperatures.[17] It must be noted that in decreasing field a weak remanent magnetization has been observed which vanishes at 12.5 K,[14,17] and

8 K,[17] respectively, for CeBi and CeSb. Therefore these magnetization measurements have permitted the determination of magnetic phase diagrams[6,13,14,17] which are quite unusual. For CeSb the phase diagram is different and much more complicated than that of CeBi.

Neutron-diffraction measurements were made on CeBi to determine the type of magnetic order which develops in this metamagnetic compound. In contrast to results obtained for polycrystalline samples[19,20] which show an antiferromagnetic structure of type I [$\vec{k}=(0,0,1)$], Cable and Koehler[21] have found with single-crystal measurements that two antiferromagnetic structures occur. The high-temperature structure develops below 25.2 K and consists of ferromagnetic (001) layers of moments in a $+-+-$ stacking sequence. At 12.5 K there is a first-order transition to the low-temperature structure which also has ferromagnetic (001) layers but in the sequence $++--$ (type IA). The intermediate-field structure has been determined by Lander *et al.*[22] The structure reported consists of a $+++-$ stacking sequence of (001) ferromagnetic planes, as first suggested by Tsuchida and Nakamura.[13] This structure exhibits a net magnetization of one half the saturated value as given by magnetic measurements. However, the phase diagram may be more complicated because all the magnetization steps[17] have not been analyzed by Lander *et al.*[22] Moreover, an important question remains about the mechanism which drives the transition between the two phases; Hullinger *et al.*[18] have observed no lattice-parameter discontinuity at the transition temperature, whereas Lander *et al.*[22] have measured a volume discontinuity of $(8\pm1)\times10^{-5}$.

For CeSb the phase diagram is much more complicated, and this work deals with the determination of the numerous magnetic field structures by neutron-diffraction experiments. In zero field the magnetic structures have been investigated by Lebech *et al.*[23] and Fischer *et al.*[24] Their neutron-diffraction measurements on single crystals of CeSb show a first-order transition to an antiferromagnetic phase at 16.0 K corresponding to the appearance of a slight tetragonal distortion of the NaCl structure.[18,25] Between T_N and 4.2 K five structures were successively observed, they consist of ferromagnetic (001) layers with the magnetic moments oriented perpendicular to the layers with a value modulated according to sine waves. The propagation vector $\vec{k}=(0,0,k)$ has in general an incommensurate value, except just below T_N ($k=\frac{2}{3}$) and at a low temperature ($k=\frac{1}{2}$), where a $++--$ sequence occurs. This structure appears at about 8.5 K, where x-ray and specific-heat measurements[18] showed an anomaly, however, Levy[25] and Busch *et al.*[26] have not observed this anomaly.

After a brief description of the experimental procedure given in Sec. II, we will compare in Sec. III the zero-field magnetic structures observed for our crystal with previous published results. The results will be analyzed in detail in order to understand why there are differences. In Sec. IV the phase diagram is reported together with a determination of the magnetic structures of the numerous phases. In Sec. V magnetization measurements are compared with neutron results and special attention is paid to the remanent magnetization behavior. An analysis and a simple thermodynamic justification of the quite original phase diagram are given in Sec. VI. In particular the nature of the phase transition observed at about 8.5 K in zero field will be discussed in order to explain why the experimental results can be different. Another important question concerns the nature of the Ce^{3+} ground state in CeBi and CeSb. In the ordered state the Ce^{3+} magnetic moments have about the full free-ion moment value ($2.10\mu_B$, see Table I) and are highly anisotropic along a fourfold axis. In contrast to these results, magnetization measurements in diluted compounds[15,27,28] show that the easy magnetization axis is a threefold axis. The crystal field splits the multiplet $J=\frac{5}{2}$ into a quartet Γ_8 and a doublet Γ_7. Inelastic neutron scattering and specific-heat measurements revealed that the $\Gamma_7-\Gamma_8$ splitting is extremely low: between 9 K (Ref. 29) and 4 K (Ref. 30) for CeBi and between 24 K (Refs. 7, 31) and 38 K (Ref. 32) for CeSb (Table I). The easy direction is $\langle001\rangle$ if Γ_8 is the ground state and $\langle111\rangle$ if it is the doublet Γ_7. So in the diluted compound the Ce^{3+} ground state is unambiguously the Γ_7 doublet. But in pure compounds and in particular in CeSb, the experiments do not allow the clear determination of the nature of the ground state. However, Wang and Cooper[11] deduce a Γ_7 ground state in order to interpret the anomalous behavior of the susceptibility. Thus Cooper and Vogt[27] proposed a strong anisotropic exchange to give a $\langle001\rangle$ magnetic-moment anisotropy. On the other hand, Hullinger *et al.*[18] observed no such susceptibility anomaly in very-low-field measurements and at T_N a tetragonal distortion occurs. This problem will be discussed in Sec. VI. Stevens and Pytte[39] give a justification of such a distortion (tetragonal rather trigonal) by a Jahn-Teller effect: The low-angular-momentum value can stabilize only a tetragonal distortion, this implies that Γ_8 becomes the ground state at the transition which is in fact split by the second-order crystal-field term.

So, as we have seen in this introduction, some unanswered questions remain and we hope that our results on CeSb will provide information to clarify the magnetic properties of monopnictide compounds.

TABLE I. Some published data for cerium monopnictides.

Compound	CeP	CeAs	CeSb	CeBi
Lattice constant at room temperature (Å)	5.909 (Refs. 2, 29)	6.072 (Refs. 2, 29)	6.412 (Refs. 2, 29) 6.4230 (Ref. 18) 6.422 (Ref. 25)	6.500 (Refs. 2, 29) 6.503 (Ref. 18)
Tetragonal distortion $(a-c)/a$			**1.10^{-3} (at 7 K) (Ref. 18)** $2.5\ 10^{-3}$ (at 4 K) (Ref. 25)	10^{-3} (at 7 K) (Ref. 18) **$<1.10^{-4}$ (Ref. 22)**
Néel temperature T_N (K)	**10 (Ref. 4)** 9 (Ref. 5) 8.8 (Ref. 33) 8 (Ref. 34)	8 (Ref. 4) 7.5 (Ref. 5)	18 (Refs. 4, 14) 16 (Refs. 5, 18, 23) 16.2 (Ref. 17)	25 (Refs. 4, 13, 18) 26 (Refs. 19, 35) 25.6 (Refs. 14, 17) 25.2 (Ref. 21)
Paramagnetic Curie-Weiss temperature T_P (K)	5 (Ref. 4) −12 (Ref. 5) 3.6 (Ref. 10)	−21 (Ref. 4) −8 (Ref. 5) +9.9 (Ref. 10)	5 (Ref. 4) 8 (Ref. 5)	12 (Refs. 4, 13)
Saturated moment in μ_B/Ce atom (free-ion value $gJ = 2.14\mu_B$)	0.8 (Ref. 36)	0.68 (Ref. 7) 0.83 (Ref. 31)	1.8 (Ref. 5) 2.05 (Refs. 12, 24) 2.11 (Ref. 17)	1.8 (Ref. 13) 2.0 ± 0.1 (Ref. 19) 2.1 (Refs. 15, 21, 22) 2.14 (Ref. 17)
Crystal-field splitting between Γ_7 and Γ_8 Δ (K)	200 (Ref. 9) 135 (at 18 K) (Ref. 29) 161 (Ref. 37)	140 ± 10 (Ref. 7) 141 ± 8 (at 290 K) (Ref. 29) 142 ± 12 (Ref. 38)	<25 (Ref. 7) 24 ± 2 (Ref. 26) 38 (at 20 K) (Ref. 32)	9 ± 3 (at 120 K) (Ref. 29) 4 (Ref. 30)
Easy magnetization axis	(100)	(100)	(100)	(100)
Magnetic order	fcc type I	fcc type I	Complex (Refs. 5, 7, 23, 24) six phases below 16 K most of them are incommensurate	Complex (Refs. 4, 19–22) two AF phases $12.5 < T < 25$ K AFM I[a] $T < 12.5$ K AFM IA[b]

[a] AFM I, antiferromagnetic order of type I: $k = (0, 0, 1)$.
[b] AFM IA, antiferromagnetic order of type IA: $k = (0, 0, \frac{1}{2})$.

II. SAMPLE AND EXPERIMENTAL PROCEDURE

The single crystal of CeSb was prepared as described by Busch and Vogt.[5] This was a pillar-shaped crystal of approximate dimensions $1\times1,5\times2.5$ mm^3 with the edges parallel to the $\langle100\rangle$ directions of the rocksalt structure. Magnetic fields were applied along the [001] direction which corresponds to the largest edge.

Magnetization measurements were performed in static fields up to 150 kOe and in the temperature range 2–25 K at the Service National des Champs Intenses at Grenoble. Magnetization curves, at constant magnetic field or constant temperature, were obtained by moving the sample between two opposed pickup coils in a homogeneous magnetic field ($\Delta H/H=4\%_0$) produced by a Bitter coil.[17,40]

Neutron-diffraction experiments were performed on the DN_3 spectrometer of the Siloe reactor at the Centre d'Etudes Nucléaires at Grenoble. This double-axis spectrometer is connected to a computer and is equipped with an elevating counter arm which allows scanning of the nonequatorial reciprocal space up to an angle of 45°. Neutrons of wavelength 1.115 Å were used for all the measurements. The crystal was put inside a cryomagnetic system which produces a magnetic field until a value of 50 kOe either with a horizontal or vertical direction.[41] The sample temperature can be adjusted between 1.5 K and room temperature. The temperature stability is better than 0.01 K in the temperature range investigated (1.5–20 K). In our experiments a vertical magnetic field was applied along the [001] axis of the crystal allowing a more accurate measurement of the ferromagnetic component.

Nuclear reflection intensities were measured in order to test the importance of extinction phenomena and to determine the scaling factor. The fcc structure gives rise to two kinds of nuclear reflections: strong reflections ($F=b_{Ce}+b_{Sb}$) with even Miller indices and weak reflections ($F=b_{Ce}-b_{Sb}$) with odd Miller indices. At the magnetic ordering an increase in the intensity of the strong reflections has been observed. For example, the (200) reflection increase by 9% when the crystal orders in a multidomain state while for a monodomain state the intensity has the same value as for the paramagnetic state. This result indicates an extinction of 9% for the strong reflections in the monodomain and paramagnetic states. Therefore, these extinction effects are negligible for a crystal in a multidomain state owing to the fact that the domain size is smaller than the size of the crystallites. So for the magnetic reflections, we can consider the extinction as negligible because their intensity are an order of magnitude smaller than the strong nuclear reflections. In these conditions, the measurements of the (200) reflection intensity in the multidomain state permits us to determine the scaling factor using the Fermi lengths in 10^{-12} cm, $b_{Ce}=0.482$ and $b_{Sb}=0.564$.[42] The intensities were internally calibrated in order to obtain absolute values which were compared to the calculated one for determining the magnitude and the direction of the magnetic moment.

The fcc structure contains only one Bravais lattice, thus the magnetic structure is completely determined by the knowledge of the Fourier decomposition

$$\vec{m}_n=\sum_{\vec{q}} m_q e^{i\vec{q}\cdot\vec{R}_n},$$

where q is restricted to the first fcc Brillouin zone. We will characterize each Fourier component by the propagation vector $\vec{k}$ such as $\vec{q}=(2\pi/a)\vec{k}$ and by an amplitude A_k. The propagation vectors $\vec{k}$ have been determined by scanning the Brillouin zone (200) along the [20l], [2k0], or [h20] directions. The experimental geometry gives a very good accuracy for the [2k0] and [h20] directions of the equatorial plane ($\Delta k_{x,y}=0.001$), whereas for the vertical direction [20l] the vertical beam divergence reduces the accuracy to $\Delta k_z=0.005$. The amplitude value A_k is determined from the superlattice reflections corresponding to a scattering vector $\vec{h}=\vec{H}\pm\vec{k}$ ($\vec{H}$ is the lattice scattering vector) with an intensity given by the expression

$$I_M(\vec{h})=(0.27)^2 f^2(\vec{h})(\tfrac{1}{4}A_k^2)\sin^2\alpha,$$

where $f(\vec{h})$ is the Ce^{3+} form factor calculated by Blume, Freeman, and Watson,[43] and α is the angle between the scattering vector $\vec{h}$ and the moment direction which is parallel to [001].

In the monodomain state the accuracy of the intensity measurements leads to an error of $\pm0.05\mu_B$ for the amplitude value A_k; whereas, in the multidomain state, the accuracy is lower by a factor 2 because the intensity is smaller and the domain distribution must be determined ($\Delta A_k=\pm0.1\mu_B$). The ferromagnetic component has been deduced from the intensity of the reflections (111) and (311) which have a weak nuclear contribution.

III. MAGNETIC STRUCTURES IN ZERO APPLIED MAGNETIC FIELD

The magnetic structures of CeSb in zero applied field have been investigated by Lebech, Fisher, and Rainford.[23] They found five different magnetic phases below $T_N=16.0$ K. For all these phases, the propagation vector is $\vec{k}=(0,0,k)$, i.e., the magnetic structures consist of (001) ferromagnetic planes with moments modulated according to sine

waves along the [001] direction. The magnetic moments are confined along the [001] direction. The value of k varies discontinuously with temperature and lies between $\frac{2}{3}$, just below T_N, and approximatively $\frac{1}{2}$ at low temperature. The five magnetic structures have been observed in the following temperature range: I: 16.0–15.4 K; II: 15.4–14.8 K; III: 14.8–12.2 K; IV: 12.2–8 K and V: ≤ 8.0 K. Higher harmonics in the modulation of the moments are present except for the commensurate phases I and V. Experiments performed on a new crystal of CeSb by Fischer, Meier, and Vogt[24] have confirmed these results, but a new phase has been observed between the phases IV and V. A pronounced hysteresis is associated to the transition between this phase and the phase $k=\frac{1}{2}$.

The results obtained with our single crystal show some differences, the main one is that we have not observed the $k=\frac{1}{2}$ phase for temperatures down to 1.7 K. Instead the magnetic structure corresponds to a propagation vector $k=0.572$, i.e., to the phase III of Lebech *et al.*[23] and Fischer *et al.*[24] When temperature is increased the results are reported in Fig. 1(a). This phase ($k=0.572$) disappears at 15.4 K, above this temperature a phase $k=0.667$ (phase I of Refs. 23 and 24) develops until 16.35 K where a transition to the paramagnetic state occurs. The superlattice reflection intensities of the structure vanish in a temperature range of only

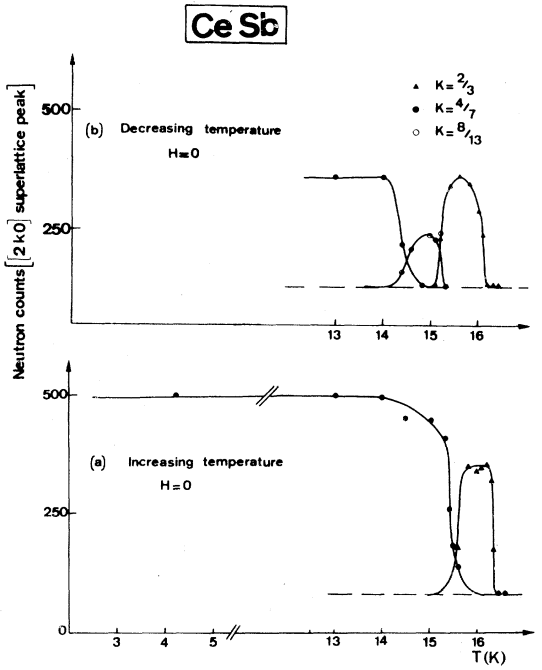

FIG. 1. Thermal variation of the intensity maximum of the $(2k0)$ superlattice peaks for CeSb.

0.06 K, indicating a first-order transition in agreement with previous work.[23,24] When the temperature is decreased [Fig. 1(b)] the phase $k=0.667$ appears at $T=16.2$ K, so a temperature hysteresis is detected at the Néel temperature. Below $T=15.3$ K a new phase $k=0.614$ occurs which corresponds to the phase II of Refs. 23 and 24. This phase was not observed with increasing temperature. The phase $k=0.572$ appears at 14.4 K and remains down to 1.78 K. However at 4.2 and 1.78 K a small contribution of a phase $k=0.55$ is present together with $k=0.572$. Therefore, in zero magnetic field, from our experimental results we can take into account only the two main phases $k=0.667$ and $k=0.572$, observed, respectively, at high and low temperature, because the phase $k=0.614$ was observed only with decreasing temperature and in a very small temperature range.

Within the experimental accuracy, the propagation vector values can be considered as fractional numbers; i.e., $k=\frac{4}{7}=0.572$, $k=\frac{8}{13}=0.615$, and $k=\frac{2}{3}=0.667$. So the magnetic structures are commensurated with the lattice; for example, $k=\frac{4}{7}$ corresponds to a magnetic cell equal to seven times the nuclear cell.

If we analyzed in detail the results of Lebech *et al.*[23] and Fischer *et al.*[24] we see that the so-called incommensurate value of the propagation vectors are in fact also fractional numbers I: $k=\frac{2}{3}$; II: $k=\frac{8}{13}$; III: $k=\frac{4}{7}$; IV: $k=\frac{5}{9}=0.555$; V: $k=\frac{6}{11}=0.547$; and VI: $k=\frac{1}{2}$. These values are not arbitrary and are given by a general formula $k=n/(2n-1)$ except the value $k=\frac{8}{13}$. The value $k=\frac{1}{2}$ corresponds to $n=\infty$.

Moreover, in addition to the magnetic superlattice peaks associated to the propagation vector $\vec{k}$, small superlattice peaks have been observed which corresponds to the third-order harmonics. In these conditions the magnetic structures of these phases can correspond to square-wave structures with a wave-vector value equal to the Fourier component associated to the more intense superlattice peak. A more detailed discussion is given in annex. Thus for $n=1,2,3,4,5,6,\ldots,\infty$ the corresponding square-wave structures are reported in Fig. 2. It can be seen that all the structures are derived from the phase $k=\frac{1}{2}$ which corresponds to a $++--$ staking sequence of ferromagnetic (001) planes. In such a structure each plane has two neighboring planes with an opposite moment direction. Let us call a "fault" in the sequence a plane which has two neighboring planes with the same moment orientation (i.e., $-+-$ or $+-+$). Thus a structure with $k=n/(2n-1)$ corresponds to a $++--$ staking sequence with a "fault" which appears periodically each n crystalline cell (hatched

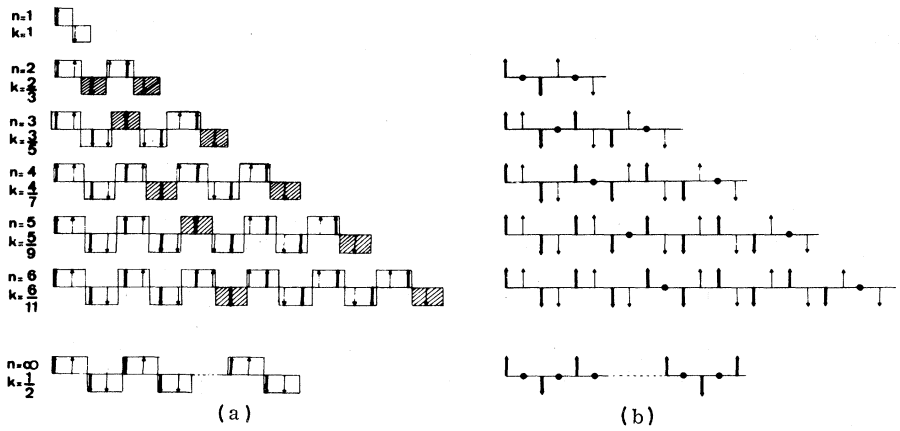

FIG. 2. Square-wave magnetic structures associated to a wave vector $k = n/(2n-1)$. (b) is obtained from (a) by a phase change of the square-wave function.

in Fig. 2). It must be noted that a crystalline cell contains two planes. For n even the "fault" plane (Fig. 2) have their magnetic moments which are parallel, so a ferromagnetic component associated to the harmonic of order $2n-1$, can exist with a magnitude $\mu/(2n-1)$ per Ce^{3+} ion. For n odd the structure is purely antiferromagnetic. However, when n is even, it is possible to cancel the ferromagnetic component by choosing conveniently the phase of the square wave (see Appendix), but in this case two ferromagnetic planes are transformed into two paramagnetic planes. The same result can be obtained for n odd. It is a special type of magnetic order that we shall call antiferroparamagnetic (AFP) (Fig. 2).

We shall examine now each phase in more detail.

Phase S_1: $k=\frac{2}{3}$. At 16 K the intensities of the magnetic supperlattice reflections have been measured for the three domains K_x, K_y, K_z associated with the propagation vector $(k,0,0)$, $(0,k,0)$, and $(0,0,k)$. We must note that they are distributed with an almost equal proportion. An amplitude value $A_k = (1.9 \pm 0.1)\mu_B$ is deduced for the sine-wave modulation. As no ferromagnetic component has been observed, the magnetic structure may be described by a square-wave structure such as to have a $+-0+-0$ stacking sequence. This problem will be discussed in more detail in Sec. VI.

Phase S_1: $k=\frac{8}{13}$. Because of the size of our crystal and the weakness of the observed intensities it was not possible to obtain quantitative measurements for this phase.

Phase S_2: $k=\frac{4}{7}$. Measurements have been done at 13 and 10 K. The results show that the intensity values and the domain distribution are about the same for the two temperatures, but the three domains are not distributed with an equal proportion (33, 42, and 35%). The amplitude of the Fourier component $k=\frac{4}{7}$ is $(2.6 \pm 0.1)\mu_B$ at 13 K and $(2.7 \pm 0.1)\mu_B$ at 10 K. These values are larger than the free-ion moment value $(2.14\mu_B)$. They are associated to the fundamental term of a square-wave modulation. In addition a third-order harmonic $(k = 0.286 = \frac{2}{7})$ is present, an amplitude $A_{3k} = (0.86 \pm 0.2)\mu_B$ has been measured at 10 K. Thus the experimental ratio A_k/A_{3k} takes the value 3.1 ± 0.3 which lies between the theoretical ones 3.5 and 2.8 associated, respectively, to a AFP and antiferro-ferromagnetic (AFF) structure (see Appendix). However, at this temperature, as will be discussed in Sec. VI, we may consider this phase as a square-wave structure with a zero net magnetization, i.e., corresponding to a $++--+0-++--+0-$ stacking sequence of ferromagnetic and "paramagnetic" (001) planes. In a ferromagnetic plane the magnetic moment of a cerium ion is given by $\mu = A_k/1.252$, i.e., $\mu = (2.15 \pm 0.1)\mu_B$ at 10 K.

In all these three phases the magnetic moments are aligned along the propagation vector, i.e., a fourfold axis.

IV. NEUTRON-DIFFRACTION INVESTIGATION OF THE MAGNETIC FIELD VERSUS TEMPERATURE PHASE DIAGRAM

The magnetic phase diagram of CeSb has been investigated by neutron-diffraction experiments at different temperatures with an increasing and decreasing magnetic field applied along a fourfold axis. The variation of the propagation vector versus magnetic field has been determined from scans along the $[20l]$ direction in reciprocal space. The phase diagrams determined with increasing and decreasing fields are reported, respectively, in Figs. 3 and 4. These phase diagrams can be divided into two zones: a low-temperature zone which contains the phases S, S', and F; a high-temperature zone which concerns the ferro-paramagnetic (FP) phases (four phases have been observed). The existence of these phases gives a quite original character to the phase diagram

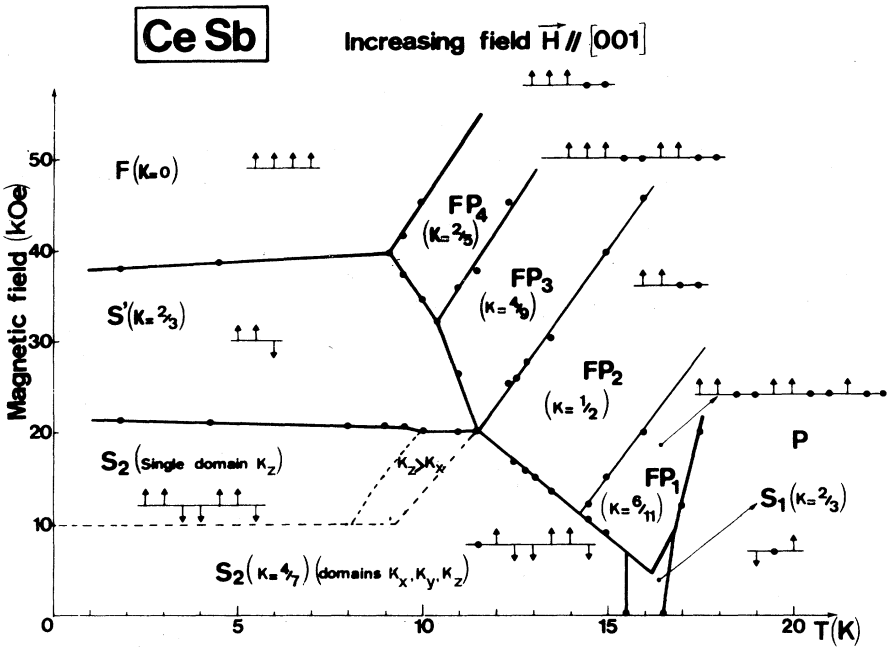

FIG. 3. Magnetic phase diagram of CeSb for an increasing field applied along a [001] direction. The dashed lines correspond to a change of the domain distribution. An arrow ↑ or ↓ represents the magnetization up or down along the z axis of a (001) plane.

which do not correspond to that of an usual metamagnet.

A. Low-temperature zone

At 4.2 K, when the magnetic field increases, the phase S_2 ($k=0.572=\frac{4}{7}$) remains stable up to a field of 21 kOe. At higher field a new phase S' appears characterized by a propagation vector $k=\frac{2}{3}$. At 20.9 kOe the coexistence of the phases S and S' indicates a first-order transition. The phase S' disappears at $H=39$ kOe and in higher field the system becomes completely saturated. Figure 5 gives the field dependence of the intensity maximum of the [20k] superlattice reflections together with the [111] integrated intensity. The critical fields show only a weak temperature dependence, however they are affected by hysteresis effects which are quite important for the $S \rightarrow S'$ phase change (about 9 kOe). These results are in good agreement with magne-

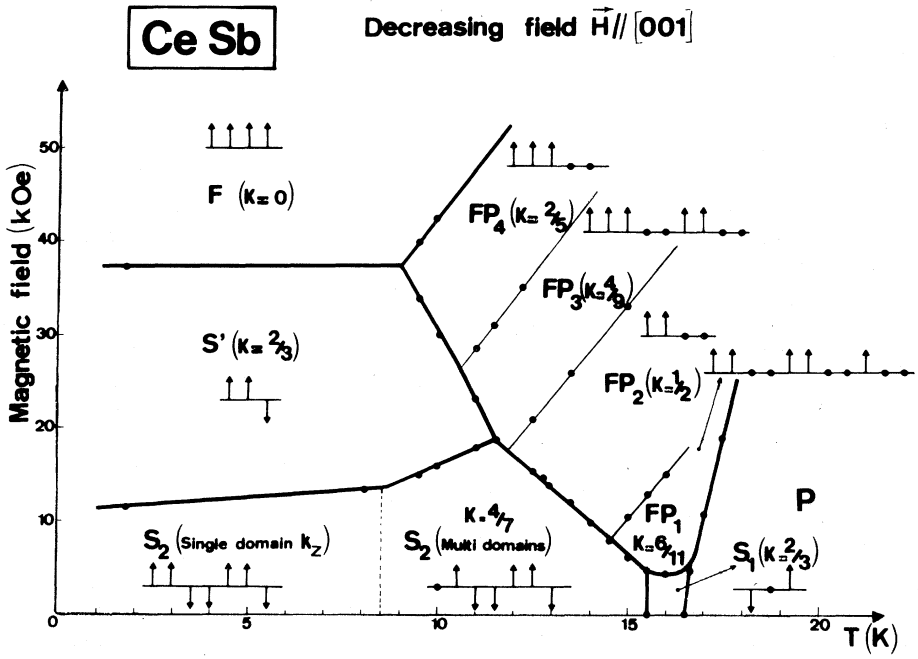

FIG. 4. Magnetic phase diagram of CeSb for a decreasing field applied along a [001] direction. An arrow ↑ or ↓ represents the magnetization up or down along the z-axis of a (001) plane.

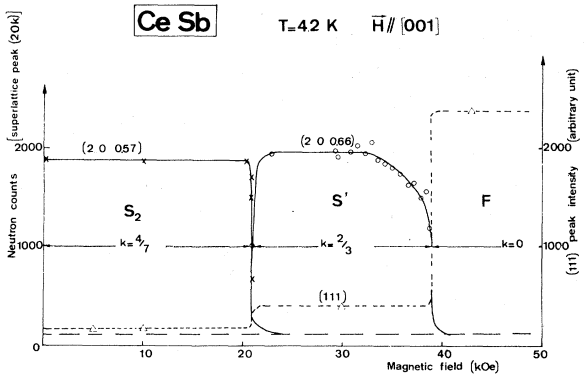

FIG. 5. Field dependence of the intensity maximum of the $(20k)$ superlattice reflections and of the (111) integrated intensity at $T = 4.2$ K.

tization results.[17]

Phase S_2. This phase corresponds to the phase S_2 observed in zero field, i.e., a square-wave structure with a propagation vector $k=\frac{4}{7}$. It corresponds to ferromagnetic (001) planes in a $++--++-$ stacking sequence.

Phase F. It corresponds to the induced ferromagnetic state ($k=0$). The intensity measurement of the weak nuclear (111) and (311) reflections lead to a magnetic moment value of $\mu_F = (2.08 \pm 0.05)\mu_B$/Ce atom. This value is very close to the free-ion value $2.14\mu_B$.

Phase S'. The value of the ferromagnetic component determined from the (111) and (311) reflection intensities is $(0.71 \pm 0.05)\mu_B$/Ce atom. In agreement with magnetization measurements this value is one third of the saturated magnetic moment value in the induced ferromagnetic state. Moreover, superlattice reflections corresponding to a propagation vector $k=\frac{2}{3}$ are observed and from the intensities of the $[20k]$, $[22k]$, and $[11\,1-k]$ a Fourier component amplitude $A_k = (2.87 \pm 0.05)\mu_B$/Ce atom is deduced (Table II). The experimental ratio of 4.04 between this amplitude and the ferromagnetic component leads to the conclusion that the magnetic structure can be described by a square wave with a propagation vector $k=\frac{2}{3}$ and an amplitude μ. Indeed, as shown in the Appendix, such a structure gives rise to two Fourier components: a fundamental term $k=\frac{2}{3}$ with an amplitude $A_k=\frac{4}{3}\mu$ and a third-order harmonic which corresponds in fact to the ferromagnetic component ($k=0$) with a value of $\frac{1}{3}\mu$. In these conditions the moment value is $\mu = \frac{3}{4}A_k = (2.15 \pm 0.05)\mu_B$/Ce atom. So the magnetic structure of the phase S' consists in ferromagnetically aligned $(00l)$ layers of moments μ in a $++-$ stacking sequence with the moment oriented along the [001] axis (Fig. 3).

B. High-temperature zone

At high temperature, four FP phases are observed: FP_1, FP_2, FP_3, FP_4. In Fig. 6 are reported scans along the $[20l]$ direction in all the (200) Brillouin zone for each phases. The most intense superlattice reflection corresponds to a Fourier component k which have the following value: $k=0.55$ for FP_1, $k=0.50$ for FP_2, $k=0.45$ for FP_3, and $k=0.40$ for FP_4.

These values have been obtained by scans along vertical directions, so the measurements are less accurate than those performed in the equatorial plane. According to an estimated error $\Delta k = 0.005$ these values can be written as fractional numbers, i.e., respectively, $k=\frac{6}{11}$, $\frac{1}{2}$, $\frac{4}{9}$, and $\frac{2}{5}$. Moreover, except for the phase FP_2 ($k=\frac{1}{2}$) a weak superlattice reflection has been observed which is associated to the third-order harmonic. It corresponds to a Fourier component $k' = 2 - 3k$. To illustrate the phase changes the variation of the $(20k)$ superlattice reflection intensities with an increasing magnetic field at $T = 11$ K is reported in Fig. 7. We observe successively the multidomain and the monodomain states of the phase S_2, then the phase S' and the phases FP_3 and FP_4. In these two last

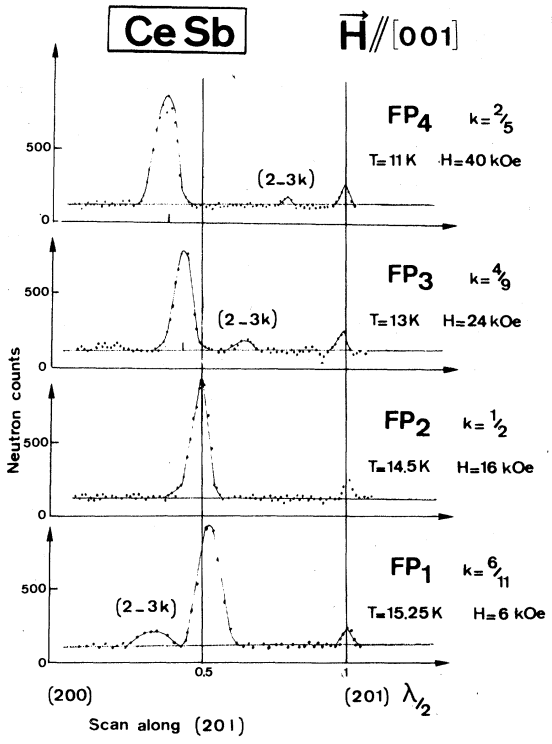

FIG. 6. Typical scans along the $[20l]$ direction in the (200) Brillouin zone for the FP phases.

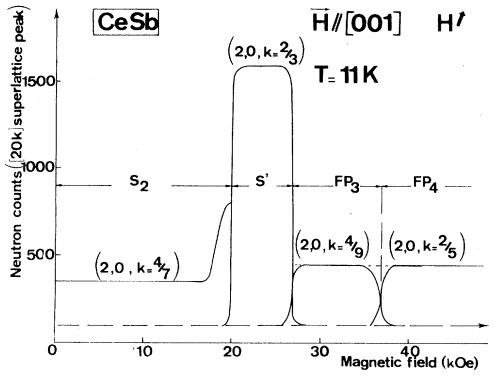

FIG. 7. Field dependence of the intensity maximum of the $(20k)$ superlattice reflections at $T=11$ K.

phases the superlattice reflection intensity is four times smaller than the intensity of the S' or S_2 (monodomain) phases. On the other hand the FP phases exhibit a large ferromagnetic component with a value of about one half the saturated magnetization. The observed values of the ferromagnetic component are reported in Table II. Therefore these structures exhibit a ferromagnetic and a modulated component. The ferromagnetic component is confined along the magnetic field, i.e., the [001] axis.

For the modulated component two hypotheses are possible:

Model A. The modulated component is parallel to the propagation vector and therefore is collinear with the ferromagnetic component. In this model every moment has the same direction but may have different magnitude.

Model B. The modulated component is located in a plane perpendicular to the propagation vector. This modulated component associated to the ferromagnetic component leads to a noncollinear structure. This model is plausible for $k=\frac{1}{2}$, indeed the magnetic moment directions, which are obtained by $\frac{1}{2}\pi$ rotation around the z axis, could take the direction of the $\langle 111\rangle$ axis. However, for the other phases (FP_1, FP_3, FP_4), the magnetic moment directions would be far from any crystallographic axis, and this is in disagreement with the strong magnetic anisotropy observed at low temperatures. By magnetic measurements, moreover, with such a model, it is difficult to understand why the propagation vector takes only discrete value. In order to choose between these two models we shall examine in detail the case of the most simple phase, i.e., the FP_2 phase.

FP_2 phase ($k=\frac{1}{2}$). *In the B model* the modulated component gives rise either to a sine-wave or a spiral structure. The sine-wave structure can be eliminated because it leads to incorrect intensities.

For the conical structure, the measured value of the spiral component is $A_K=(1.38\pm0.05)\mu_B$ (Table II) which, taking into account of the ferromagnetic component $\mu_F=(1.08\pm0.05)\mu_B$, gives a moment value of $(1.74\pm0.08)\mu_B$. This value is smaller than the measured values in zero field: $2.1\mu_B$ at 4.2 K. Moreover, the spiral component value deduced from the $[11\frac{1}{2}]$ reflection intensity has a low value which cannot be explained by the experimental accuracy.

A model. For the A model the amplitude of the modulated component is $A_k=(1.47\pm0.05)\mu_B$ (Table II). Combined with the ferromagnetic component $\mu_F=1.08\mu_B$ it leads to a stacking sequence of (001) ferromagnetic planes for which the moment value varies according to the following relation:

$$\mu_{Ce}=1.08+1.47\sin(n\tfrac{1}{2}\pi+\gamma)\,.$$

If the phase γ takes any value, a plane n containing moments with a value of $(2.55\pm0.1)\mu_B$ will exist. This situation is impossible because the maximum value of a cerium moment is $2.14\mu_B$. To satisfy this condition the phase must be equal

TABLE II. Moment values associated to each phase. μ_F is the net ferromagnetic component, A_k is the amplitude of the most intense Fourier component, μ_{sw} is the value of the square-wave amplitude, and μ_{Ce} is the moment of a cerium ion in a ferromagnetic plane.

Phases	H (kOe)	T (K)	μ_F (μ_B)	A_k (μ_B)	μ_{sw} (μ_B)	μ_{Ce} (μ_B)
F: $k=0$	43	4.2	2.08	•••	•••	2.08 ± 0.05
S': $k=\frac{2}{3}$	30	4.2	0.71	2.87	2.15	2.15 ± 0.05
FP_1: $k=\frac{6}{11}$	10	15.5	0.76	1.26	0.99	1.84 ± 0.1
FP_2: $k=\frac{1}{2}$	43	16.0	1.08	A: 1.47	1.03	2.11 ± 0.1
				B: 1.38	•••	1.74 ± 0.1
FP_3: $k=\frac{4}{9}$	43	13.0	1.24	•••	•••	
FP_4: $k=\frac{2}{5}$	40	11.0	1.33	1.33	1.03	2.16 ± 0.1

to $\frac{1}{4}\pi$, thus the modulated component corresponds to a $++--$ square-wave structure with an amplitude $\mu_{sw}=(1.03\pm0.05)\mu_B$ (Table II). We must note that this value is pratically equal to the ferromagnetic component ($1.08\mu_B$). Therefore, the combination of these two components gives an original magnetic order consisting in two (001) ferromagnetic planes with $\mu_{Ce}=2.11\pm0.1\mu_B$ followed by two (001) planes with a zero average magnetization [$\mu_{Ce}=(0.05\pm0.1)\mu_B$] which we call "paramagnetic." We must note that the moment value in the ferromagnetic plane ($2.11\mu_B$) is in good agreement with the value determined in the ferromagnetic region or in the magnetic states observed in zero field. This type of structure is quite original and for convenience we call it ferro-paramagnetic (FP). This A model is compatible with the experimental accuracy and is better than the B model. However, it is possible to consider another model. The value of the ferromagnetic component, one half of the saturated moment, could be explained, as in CeBi,[22] by a structure with a $+++-$ stacking sequence. Nevertheless, this structure gives rise to three Fourier components with wave vectors $k=0$, $k=\frac{1}{2}$, and $k=1$ with the amplitude $\frac{1}{2}\mu$, μ, and $\frac{1}{2}\mu$ respectively. As no superlattice reflections associated to $k=1$ have been observed this model must be eliminated. Finally the A model is the most adequate model and the structure corresponds to a periodic arrangement of two ferromagnetic planes followed by two paramagnetic planes ($+-00$).

FP_4 phase ($k=\frac{2}{5}$). As for the FP_2 phase, the conical model must be eliminated on account of the low-intensity values. Moreover, for the FP_4 phase additional arguments eliminate this model. First, the propagation vector value $k=\frac{2}{5}$ is not compatible with the large cubic anisotropy and secondly the presence of the third-order harmonic can be interpreted only as a squaring up of a sine-wave structure. In these conditions only the A model must be retained and from the observed reflection intensities an amplitude value $A_k=(1.33\pm0.05)\mu_B$ is deduced for the Fourier component $k=\frac{2}{5}$ (Table II). The reflection intensity due to the third-order harmonic indicates that the modulated component is a square wave with an amplitude μ_{sw}. In the case of a total squaring μ_{sw} is related to A_k by the relation $A_k=1.294\mu_{sw}$ (see Appendix), so $\mu_{sw}=(1.03\pm0.05)\mu_B$. This square-wave component gives a ferromagnetic contribution of $\frac{1}{5}\mu_{sw}=0.2\mu_B$/Ce atom (fifth-order harmonic) and in fact the net ferromagnetic component $(1.33\pm0.005)\mu_B$ is the sum of this contribution $0.2\mu_B$ and a ferromagnetic contribution of $(1.13\pm0.05)\mu_B$.

The magnetic structure is given by the combination of this ferromagnetic component and the square wave with an amplitude μ_{sw} which corresponds to a $+++--$ stacking sequence of ferromagnetic (001) planes. So the magnetic structure can be described by a periodic arrangement of three ferromagnetic planes with a moment value $\mu=(2.16\pm0.1)\mu_B$/Ce atom followed by two planes which can be considered as paramagnetic [$\mu=(0.1\pm0.1)\mu_B$]. As for the FP_2 phase the moment value of the ferromagnetic plane corresponds to the saturation value.

Therefore, the two phases FP_2 and FP_4 are represented, respectively, by the following arrangement $++00+-00$ and $+++00+++00$. Each FP phase can be described with this model which consists of the superposition of a ferromagnetic component and a square wave with about the same amplitude.

FP_3 phase. The FP_3 phase, characterized by a propagation vector $k=\frac{4}{9}$, corresponds to a $+++00++00$ stacking sequence of (001) planes. If μ is the moment value in a ferromagnetic plane, the total ferromagnetic component is equal to $\frac{5}{9}\mu$, i.e., $1.17\mu_B$ by taking $\mu=2.1\mu_B$. This value is in good agreement with the experimental one of $(1.23\pm0.05)\mu_B$.

FP_1 phase. The FP_1 phase can be classified in the same type of structure, but in this case the propagation vector $k=\frac{6}{11}$ has a value higher than $\frac{1}{2}$ and the net ferromagnetic contribution [$\mu_F=(0.76\pm0.05)\mu_B$] is lower than $\frac{5}{11}$ times the saturated value ($0.95\mu_B$). In order to clarify this fact, superlattice reflections have been measured at $H=10$ kOe and $T=15.7$ K. The amplitude value of the first-order harmonic is $A_k=(1.26\pm0.05)\mu_B$ (Table II). The squaring up of the modulation is evidenced by the presence of the third-order harmonic which has an amplitude value $A_{3k}=(0.46\pm0.03)\mu_B$. For a complete squaring up the ratio of the first- to the third-order harmonic is theoretically 2.92 (see Appendix). In this case, taking $A_k=1.26\mu_B$, the value $A_{3k}=0.43\mu_B$ is deduced, which is in good agagreement with the experimental one, $(0.46\pm0.03)\mu_B$. So this structure results in the combination of a ferromagnetic component μ_0 and a square wave characterized by a propagation vector $k=\frac{6}{11}$ and an amplitude $\mu_{sw}=Ak/1.278=(0.99\pm0.05)\mu_B$. This modulation gives a ferromagnetic contribution of $\mu_{sw}/11=0.09\mu_B$, which can be parallel or antiparallel to the ferromagnetic component μ_0.

If we add the square wave ($\mu_{sw}=0.99$) to the ferromagnetic component ($\mu_0=0.76-0.09=0.67\mu_B$), the structure would contain ferromagnetic (001) planes with magnetic-moment values equal to $+1.66\mu_B$ and $-0.32\mu_B$. The value of $1.66\mu_B$ is low compared to the value observed in zero field, and the magnetic moment value in the so-called paramagnetic planes is larger than those for the high-

field FP phases. These reasons lead us to suppose that the net magnetization results in the subtraction of the two contributions. In this case, the ferromagnetic component μ_0 is equal to $(0.85 \pm 0.05)\mu_B$, and the moment value associated to the ferromagnetic and to the paramagnetic plane is, respectively, $(1.84 \pm 0.1)\mu_B$ and $(0.14 \pm 0.1)\mu_B$. These values are consistent with the zero- and high-field ones. So the magnetic structure is described by a periodic arrangement of ferromagnetic and paramagnetic (001) planes with the stacking sequence $(++00++00+00)$. In this case the number of paramagnetic planes is higher than the number of ferromagnetic planes, in contrast with the high-field FP phases. The magnetic moments are not saturated and compensation is not complete in the paramagnetic planes.

Finally the conical model is definitively eliminated because this type of FP structures alone are able to describe both the magnetization steps and the fractional value of the propagation vector. The existence of these different FP phases can be understood by a decrease in the number of paramagnetic planes when the field increases.

C. Detailed analysis of the high-temperature and low-field phase diagram

In order to define more precisely the transition between the FP_1 phase and the S phases a more accurate phase diagram has been determined from measurements at constant field and variable temperature. In Figs. 8 and 9 are reported the phase diagrams obtained in increasing and decreasing temperature. In low field ($H < 4$ kOe), the zero-field phases are observed: $S_2 \rightarrow S_1 \rightarrow P$, when T increases, and $P \rightarrow S_1 \rightarrow S_1^* \rightarrow S_2$, when T decreases. For higher-field values the FP phases are observed; for $H < 10$ kOe there is only the FP_1 phase whereas for $H > 10$ kOe the FP_2 and FP_1 phases are successively observed.

It must be noted that a ferromagnetic component appears at $H = 4.2$ kOe and $T = 16.3$ K and that the FP_1 phase terminates in a point in the S_1 phase.

Important hysteresis effects are associated with the phase change. We must note that the hysteresis observed at constant field and variable temperature corresponds to the hysteresis observed at constant temperature and variable field. So from the phase diagram at constant field it is possible to determine those at constant temperature. To do this we must consider that the critical fields are determined by the transition line which gives the highest-field value when the field increases and the lowest value when the field decreases, so the hysteresis value is maximum.

In decreasing temperature from the paramagnetic state, a mixed phase with an order which is not well established is observed before the FP_1 phase (Fig. 10). This mixed-phase zone tends to disappear when the field increases and moreover the hysteresis observed between this phase and the

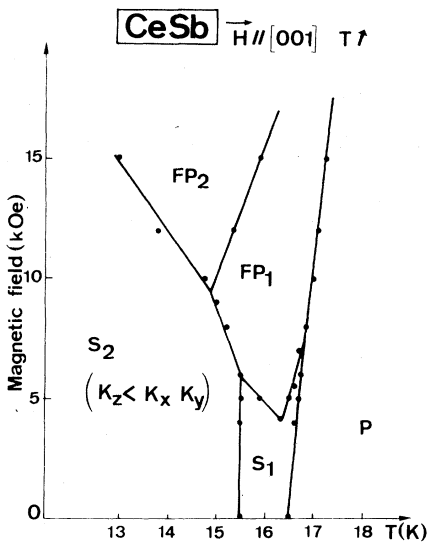

FIG. 8. Low-field and high-temperature phase diagram of CeSb in increasing temperature with field applied along the [001] direction.

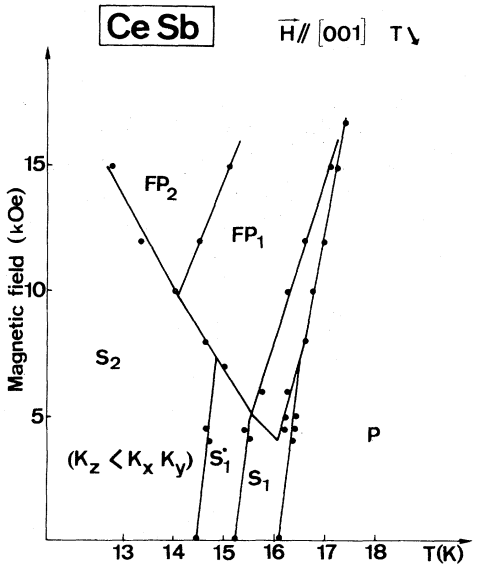

FIG. 9. Low-field and high-temperature phase diagram of CeSb in decreasing temperature with field applied along the [001] direction.

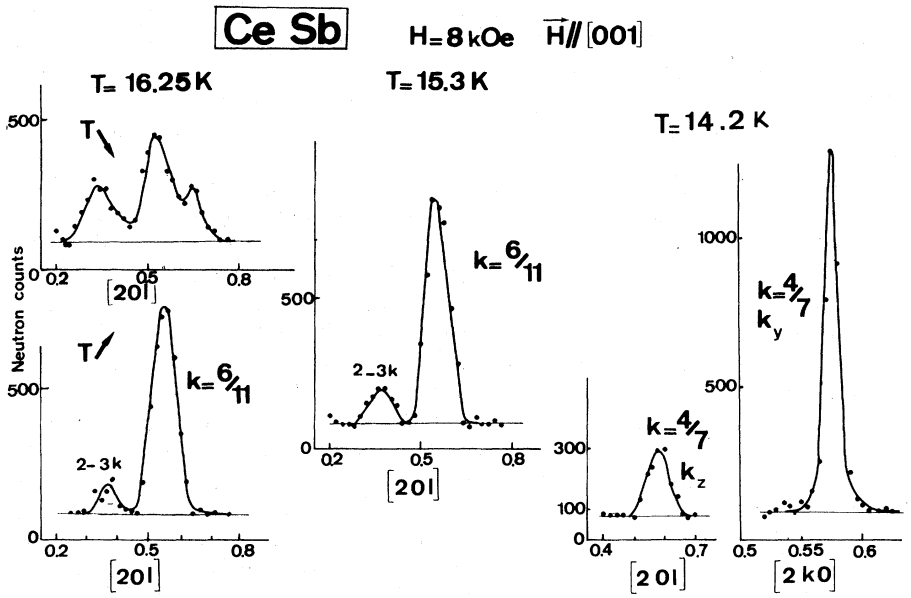

FIG. 10. Scans along the [20l] and [2k0] directions at several temperatures for a field of 8 kOe applied along the [001] direction.

paramagnetic state decreases and disappears completely above 15 kOe, which may indicate a change of the transition order. It must be noted that the ordering temperature increases linearly with the applied field.

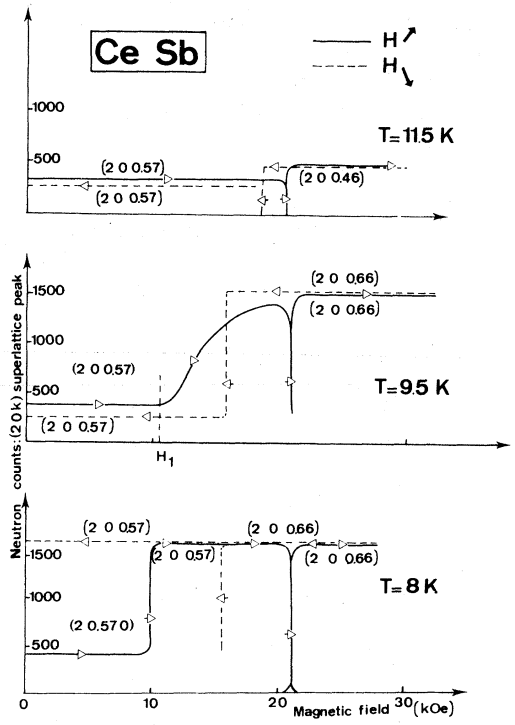

FIG. 11. Field dependence of the intensity maximum of the (20k) superlattice reflections at several temperatures in increasing and decreasing fields.

D. Domain motion study

In Sec. III we have shown that in zero field the three types of domain K_x, K_y, K_z exist in about the same proportion. In an applied magnetic field the domain motion behavior (Fig. 11) must be considered in three temperature ranges.

At low temperatures ($T \leq 8$ K) when the field increases an abrupt change from a multidomain state to a monodomain state is observed which corresponds to the domain K_z (the z direction is parallel to the field) with the same propagation vector $k = \frac{4}{7}$. The critical field line is indicated as dashed line in Fig. 3. In decreasing field the monodomain state remains down to $H = 0$.

At high temperature ($T \geq 11.5$ K) in increasing field, the multidomain distribution remains unchanged up to the transition towards the FP phases, whereas in decreasing field from the FP phases a higher proportion of K_x and K_y domains is observed. This result indicates that the perpendicular susceptibility is higher than the parallel one in this temperature range.

Between 8 and 11.5 K, when the field increases the initial multidomain state remains up to a field H_1 (Fig. 11); above this field the K_z domain proportion increases progressively up to a monodomain state S_2 or S'. In decreasing temperature a multidomain state is observed but with a higher proportion of the K_z domain.

V. MAGNETIZATION MEASUREMENT RESULTS

The first magnetic phase diagram of CeSb obtained from magnetization measurements has been given by Tsuchida *et al.*[6] using their own results

and those of Busch *et al.*[5,12] Recently, a detailed phase diagram has been published by Bartholin *et al.*[17] The phase diagram reported in this paper has been obtained from magnetization versus decreasing field curves, so it must be compared with the neutron phase diagram obtained in the same conditions (Fig. 4). The main transition lines are in good agreement except at low field and low temperatures, close to the Néel temperature and in the FP zone. However some of these disagreements are quite understandable. For example, in the FP zone the values of the magnetization of each FP phase determined by neutrons are very close ($\mu_{obs}/\mu_{satur} = 0.46, 0.5, 0.58, 0.6$, respectively, for the FP_1, FP_2, FP_3, and FP_4 phases). In order to compare the magnetization and the neutron-diffraction measurements in the FP zone a detailed magnetization curve used by Bartholin *et al.* to determine their phase diagram[17] is reported in Fig. 12. This magnetization curve has been obtained at 13 K in increasing field. Two small magnetization steps can be detected between 15 and 61 kOe which correspond to the FP phase changes: $FP_2 \rightarrow FP_3$ and $FP_3 \rightarrow FP_4$, respectively, at 29 and 52 kOe in agreement with neutron-diffraction measurements. It was difficult before the neutron-diffraction results to associate these small steps with phase changes. The authors[17] report in the FP zone a magnetization value of one half the saturation one in agreement with the average value obtained by neutron-diffraction results.

Likewise, the phase $S_1 (k = \frac{2}{3})$, close to the Néel temperature, cannot be observed with magnetization measurements. At low temperature and low field a transition line which intercepts the temperature axis at 7.5 K has been reported. We think that it corresponds to a phase change (AFF → AFP) as discussed in Sec. VI. Below this temperature a remanent magnetization was observed which disappears below 4.2 K. Below this temperature, in zero field the magnetic structure may be that observed by Lebech *et al.*[23] and Fischer *et al.*[24] (++−−++−−). The hysteresis effects are of the same magnitude as those observed by neutron-diffraction measurements.

In order to compare directly the neutron-diffraction and the magnetic measurements we have made magnetic measurements with the single crystal used for neutron-diffraction experiments.

The magnetization curves at 4.2 K (Fig. 13) have been obtained in increasing field from the virgin state and in decreasing field from the saturated state. In increasing field the first transition at 7.8 kOe corresponds to the change from the multidomain structure of the phase S_2 $(k = \frac{4}{7})$. The measured magnetic moment in this phase is practically $\frac{1}{7}$ the saturated moment in agreement with neutron-diffraction results. The transition between the phase S_2 $(k = \frac{4}{7})$ and S' $(k = \frac{2}{3})$ occurs at 21 kOe. The magnetization in the latter phase is one third the saturated moment as shown by neutron diffraction. Then, at 38.5 kOe, the ferromagnetic state is reached. In decreasing field, the same transitions are observed but with large hysteresis effects. Moreover, the monodomain state in the phase S_2 $(k = \frac{4}{7})$ remains down to $H = 0$, in agreement with neutron results. It must be noted, that at low field and low temperature, the various crystals show different behavior.[5,6,12,17,23,24] In this range of temperature the magnetic structure must be very sensitive to the crystal quality.

The thermal variation of the remanent magnetization in zero field is given in Fig. 14. When the temperature is decreased from the paramagnetic state no magnetization is detected. However, at low temperature, an applied field induces a net magnetization which disappears at about 7.5 K when the temperature increases. These results

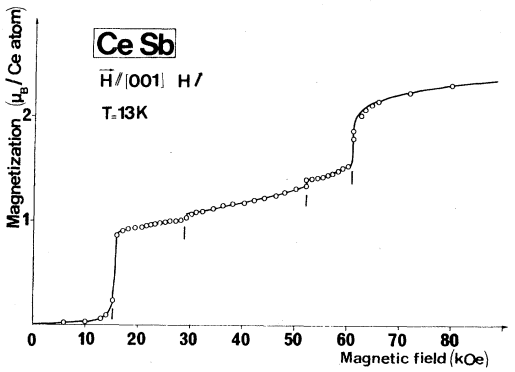

FIG. 12. Magnetization versus field at $T = 13$ K. Increasing field was applied along a [001] direction.

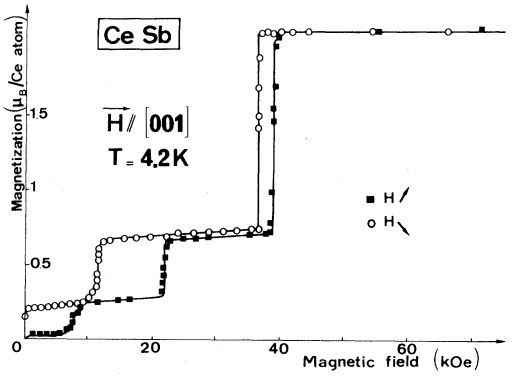

FIG. 13. Magnetization versus field at $T = 4.2$ K. The field was increased from the virgin state and decreased from the saturated state.

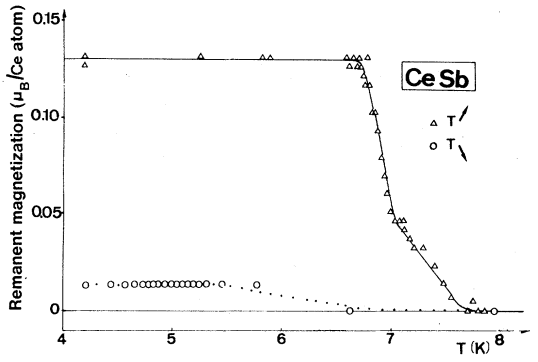

FIG. 14. Thermal variation of the remanent magnetization in increasing and decreasing temperature at $H=0$.

will be discussed in Sec. VI.

So magnetization measurements agree quite well with neutron results; the differences mentioned at low temperature may be attributed to the crystal purity. Nevertheless, whatever the purity a transition occurs between 7 and 8 K.

VI. DISCUSSION

The (H, T) phase diagram of CeSb seems, at first sight quite complicated owing to the number and the nature of the magnetic structures which have been observed. However, these magnetic structures can be described in a simple manner. They are characterized by a propagation vector which is always parallel to a fourfold axis [001] and by a strong magnetic anisotropy which confines the moment direction along the propagation vector. They consist of a periodic packing of zero magnetization planes P and ferromagnetic planes with magnetization parallel $M\uparrow$ or antiparallel $M\downarrow$ to the magnetic field. In these conditions three types of magnetic structure can be distinguished: First, the low-temperature phases with magnetic structures containing only $M\uparrow$ and $M\downarrow$ planes. We call this type of ordering antiferro-ferromagnetic (AFF). Second, at high-temperature and low field, $M\uparrow$, $M\downarrow$, and P planes coexist in the magnetic structures. This arrangement is called antiferro-paramagnetic type (AFP). Third, the magnetic structures of the high-temperature and high-field phases which contain $M\uparrow$ and P planes. The order in these structures is called "ferro-paramagnetic" (FP).

Low-temperature structures. For the low-temperature range, when the field increases the number of $M\uparrow$ planes increases discontinuously. In increasing field we observed successively the phase S_2 (++ − −++ −++ − −++ −), the phase S' (++ −++ −), and the induced ferromagnetic phase. This behavior is characteristic of a metamagnet with a high anisotropy. It corresponds to an Ising model, and the critical-field values depend on the magnetic interactions and are therefore practically temperature independent as shown from the experimental results.

Low-field and high-temperature structures. We have shown that the phase S_1, observed in weak field just below T_N, gives rise to only one Fourier component $k=\frac{2}{3}$, so this structure corresponds to a stacking of ferromagnetic (001) planes with a moment sequence along the c axis described by the general expression

$$\mu_z(z_n)=A_k \sin(2\pi k z_n+\phi),$$

where

$$z_n=\tfrac{1}{2}n \quad (n \text{ is the plane label}),$$

so

$$\mu_z(n)=A_k \sin(\tfrac{2}{3}\pi n+\phi).$$

If ϕ takes an arbitrary value, the structure is a pure sine wave one, and the moment can have any value between $-A_k$ and $+A_k$, so the amplitude A_k must be smaller than the maximum moment value $\mu_{Ce}=2.1\mu_B$.

However, a special choice of the phase ϕ gives two types of structures corresponding to

$$\phi=0 \ (+\mu, -\mu, 0, +\mu, -\mu, 0) \tag{1}$$

with $\mu=\frac{1}{2}\sqrt{3}\,A_k$

$$\phi=\tfrac{1}{2}\pi \ (+\tfrac{1}{2}\mu, +\tfrac{1}{2}\mu, -\mu, +\tfrac{1}{2}\mu, +\tfrac{1}{2}\mu, -\mu) \tag{2}$$

with $\mu=A_k$. The structure (2) must be eliminated because it is possible to change continuously this structure into the structure S' ($k=\frac{2}{3}$; ++ −) without changing the phase and thus it is hardly compatible with the fact that the phases S_1 and S' are quite separated in the phase diagram (Figs. 3 and 4). The structure (1), which corresponds to an AFP ordering, cannot be distinguished experimentally from a pure sine wave one because at this temperature the amplitude value $A_k=1.9\mu_B$ is smaller than $\mu_{Ce}=2.1\mu_B$. However the structure (1) (+ − 0 + − 0) is the most probable because we shall show that the lower-temperature phase S_2 ($k=\frac{4}{7}$) corresponds also to an AFP ordering.

For the phase S_2 ($k=\frac{4}{7}$) at high temperature ($T>8$ K) the magnetic order consists of a square-wave structure with a zero remanent magnetization, whereas below 8 K the same structure exhibits a remanent magnetization as proved by magnetization measurements (Sec. V). The cancellation of the ferromagnetic component without a change of the propagation vector corresponds to a phase change of the square wave in order to transform a ferromagnetic

plane into a paramagnetic plane (see Appendix). This type of structure AFP ($k=\frac{4}{7}$) is also supported by the fact that it permits the understanding of the difference in the domain behavior at low and high temperature. At low temperature ($T<8$ K) a noncompensated ferromagnetic plane exists which involves a strong parallel susceptibility. However at high temperature the zero net magnetization implies that the perpendicular susceptibility is higher than the parallel susceptibility and so, as has been observed, the population of K_x and K_y domains is greater than that of K_z domains, Figs. 10 and 11. Therefore we can say that, in zero field, a transition exists at about 8 K between a AFP phase S_2 $(++--+0-++--+0-)$ and a AFF phase S_2 $(++--++-++--++-)$. At this transition an entropy variation must occur which has been in fact observed by Hulliger *et al.*[18] by specific-heat measurements. We must note that this variation will be smaller as the propagation vector is nearer $\frac{1}{2}$. These authors detect also a small lattice parameter variation at this temperature. This analysis is compatible with the results of Lebech *et al.*[23] and Fischer *et al.*,[24] who also indicate such a transition at about 8 K. We think that this transition is a AFP → AFF transition though some differences exist in the results which can be attributed to the crystal quality. This conclusion is supported by the fact that in the low-temperature phase $k=\frac{1}{2}$ all planes have a magnetization whereas the high-temperature structures permit the presence of some paramagnetic planes. Moreover, the successive fractional values, observed for the propagation vector when the temperature decreases, correspond to a decrease of the number of paramagnetic planes. For our crystal the structure remains quenched with the propagation vector $k=\frac{4}{7}$. Though at low temperature the propagation vector is not $k=\frac{1}{2}$, as the other authors, the transition temperature has about the same value (~8 K) which corresponds to about $\frac{1}{2}T_N$. This behavior is to be compared with that of CeBi which exhibits at $\frac{1}{2}T_N$ a first-order transition between the low-temperature phase $(++--++--;\ k=\frac{1}{2})$ and the high-temperature phase $(+-+-;\ k=1)$.[21]

High-temperature and high-field structures. In the high-temperature and high-field range, the neutron experiments have shown clearly at least four phases of FP type which exhibit a resulting magnetization close to one half the saturated magnetic moment. These results explain the difficulty of observing these different phases by magnetization measurements.[17] However, a detailed analysis of the magnetization curves permits us to detect small magnetization steps associated with transitions between phases FP. When the magnetic field increases the phases FP_1, FP_2, FP_3, FP_4, and F occur successively. These successive phase changes correspond to a decrease in the number of paramagnetic planes when the field increases. Calling x the proportion of paramagnetic planes P. Thus, for the phase FP_2, $x=\frac{1}{2}$, whereas for the phase FP_1 $x>\frac{1}{2}$, and $x<\frac{1}{2}$ for the phases FP_3 and FP_4. In fact, these magnetic structures correspond to sequences which can be deduced from one to each others. Consider the intermediate phase FP_2 $(k=\frac{1}{2})$ which is described by a periodic arrangement of two ferromagnetic planes followed by two paramagnetic planes $(++00++00)$. At high field the observed phases FP_3 and FP_4 can be described always with a sequence $++00$ but after each n cells ($2n$ planes) appears an additional ferromagnetic plane which creates a "fault" composed of three successive ferromagnetic planes. The FP_3 phase $(k=\frac{4}{9})$ corresponds to the sequence $(+++00++00+++00++00)$. Thus, the propagation vector is given by the following relation, $k=n/(2n+1)$ and the alone possible values of k correspond to even n. Therefore, the successive possible values of the propagation vector k are

$$k=\tfrac{2}{5},\tfrac{4}{9},\tfrac{6}{13},\ldots,\tfrac{1}{2},$$

in agreement with the experiment. It is not excluded that close to the phase FP_2 $(k=\frac{1}{2})$ additional phases exist with propagation vectors $k=\frac{6}{13},\frac{8}{17}$, etc. However, highest values of n are limited by the interaction ranges. This point has not been measured in detail.

In low field the magnetic structures are obtained from FP_2 in removing a ferromagnetic plane after n cells. Thus, the propagation vector is given by the relation $k=n/(2n-1)$, where k take only even n values. Therefore the possible values of k are: $k=\frac{1}{2},\ldots,\frac{6}{11},\frac{4}{7},\frac{2}{3}$. For example, the phase FP_1 corresponds to $k=\frac{6}{11}$. The structures with $k=\frac{4}{7}$ and $\frac{2}{3}$ have not been detected, but they may be localized close to T_N where a mixture of phases is observed (Fig. 10). As previously, it is not excluded that there are, close to the phase FP_2 $(k=\frac{1}{2})$, phases with a propagation vector higher than $\frac{6}{11}$. The structures of the phases FP with $k=n/(2n-1)$ are nearly identical to those observed in zero field. The difference is only a transformation of $M\downarrow$ planes in paramagnetic planes when the field is applied.

This phase diagram is quite unusual and we must remark that on one hand the boundary between the phases FP are practically parallel straight lines and on the other hand the magnetization processes can be described by a simple "all or nothing" mechanism which consists either to a flip of $M\downarrow$ planes or to an ordering of paramagnetic planes. In order to understand the features of the phase diagram we will present a simple thermodynamic

analysis.

Simple thermodynamic analysis of the phase diagram. We assume that the magnetic states of the crystal can be described by two types of (001) planes: First, we consider ferromagnetic planes with magnetic moments parallel $M\uparrow$ or antiparallel $M\downarrow$ to the applied field. Their magnetic energy per Ce^{3+} ion will be $E = \pm\mu H - E_F$. In this relation, μ is the magnetic moment of the Ce^{3+} ion, H is the applied magnetic field, and E_F the interaction energy inside a plane. The entropy of these ordered planes is assumed to be zero. Second, we consider paramagnetic planes (P) which have a zero exchange energy and a given entropy S_0 per Ce^{3+} ion.

If x is the proportion of paramagnetic planes in the structure, y is the proportion of $M\uparrow$ planes with respect to the magnetized planes, and N is the total number of planes, the structure can be described by the number of paramagnetic planes Nx, the number of $M\uparrow$ planes $N(1-x)y$ and the number of $M\downarrow$ planes $N(1-x)(1-y)$.

The free energy per Ce^{3+} ion is given by

$$F = -xS_0T - \mu(1-x)(2y-1)H - A_k(x,y),$$

where $A_k(x,y)$ corresponds to the total exchange energy associated with the structure of propagation vector k. The free energy of the paramagnetic state $P(x=1, y=0)$ is

$$F_p = -S_0T,$$

the free energy of the ferromagnetic state $F(x=0, y=1)$ is

$$F_F = -\mu H - A(0,1),$$

and the free energy of the antiferromagnetic state $AF(x=0, y=\frac{1}{2})$ is

$$F_{AF} = -A(0, \tfrac{1}{2}).$$

As discussed previously, at high temperature and at high field, the magnetic structures of CeSb can be described by ferroparamagnetic arrangements FP corresponding to $y=1$ and x can take intermediate values between 0 and 1. First, consider the theoretical case where only the FP_2 phase ($k=\frac{1}{2}$) exists. It corresponds to $x=\frac{1}{2}$ and $y=1$. The free energy of this phase is

$$F_{FP_2}(\tfrac{1}{2},1) = -\tfrac{1}{2}S_0T - \tfrac{1}{2}\mu H - A_{1/2}(\tfrac{1}{2},1).$$

This phase is stable with respect to the P, F, and AF states if

$$F_{FP_2} < F_P: \quad \mu H + 2A(\tfrac{1}{2},1) > S_0T,$$

$$F_{FP_2} < F_F: \quad S_0T + 2A(\tfrac{1}{2},1) > \mu H + 2A(0,1),$$

$$F_{FP_2} < F_{AF}: \quad S_0T + \mu H + 2A(\tfrac{1}{2},1) > 2A(0,\tfrac{1}{2}).$$

The first two relations are possible if $2A(\frac{1}{2},1) > A(0,1)$ (this condition is not very restrictive for an antiferromagnetic system). The stability range of the different phases are reported in Fig. 15 where it can be seen that it is possible to have a FP structure stable at high temperature and high field. This result is in agreement with the observed experimental behavior. On the other hand, at low temperature all planes are ordered, $x=0$, thus the free energy does not depend on T and the transition fields between the phases AF and F are temperature independent. The transition fields are characteristic of the different exchange energies between the planes. Whereas between the phases P, FP and F we note an entropy variation and a strong variation of the transition field with temperature. The calculation shows that in the (H, T) phase diagram the transition lines between the phases P and FP as FP and F are parallel straight lines with a slope $dH/dT = S_0/\mu$, in agreement with the experimental phase diagram. The transition line between the phases AF and FP has a slope $dH/dt = -S_0/\mu$.

In reality the phase diagram is more complex perhaps due to the nature of the interactions. However, our simple model can be used to define the different transitions lines observed in CeSb. The energy of each phase can be written as a function of x and y and compared with the energy of each neighboring phases in order to obtain a theoretical expression of the transition lines in the (H, T) space. With each value of the propagation vector are associated specific values of x and y which are reported in Table III. The lack of knowledge of the interactions permits one to interpret the slopes of the transition lines which depend only on S_0/μ in our simple model. The calculated values are reported in Table IV, together with the experimental ones determined in increasing field. These values are indicative because they depend on the definition of the critical field and the value was not determined with a high accuracy. The critical

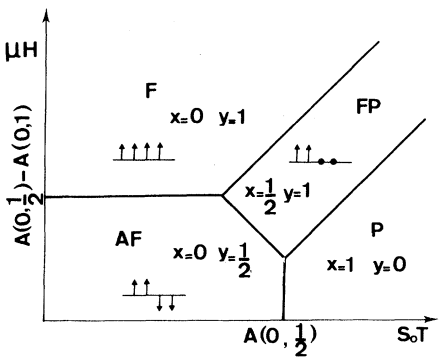

FIG. 15. Theoretical phase diagram obtained from the simple thermodynamic analysis given in Sec. VI.

TABLE III. Relation between the propagation vector and the proportion of P planes and $M\uparrow$ planes.

Phases	FP: $k=n/(2n\pm1)$	AFP: $k=n/(2n-1)$	AFF: $k=n/(2n-1)$	F: $k=0$
x	k	$(2n-1)^{-1}$	0	0
y	1	$\frac{1}{2}$	k	1

fields between AFF phases are practically temperature independent because as all the planes are magnetized there is no entropy variation. Between the phases FP all the transition lines are parallel with a slope S_0/μ. The experimental values $S_0/\mu = 6\pm1$ kOe/K and $\mu = 2.1\mu_B$ give $S_0/\mu = 0.84\pm0.15$. Thus the entropy of a Ce^{3+} ion in a paramagnetic plane can be taken as $k\ln2$ within the experimental accuracy. Using this value the calculated slopes, given in Table IV, account for the experimental results. So for the transitions $FP_1 \rightarrow AFP(S_2, k=\frac{4}{7})$ the slopes are negative with an absolute value lower than S_0/μ; whereas for the transitions $FP_3 \rightarrow AFF$ (S', $k=\frac{2}{3}$) and $FP_4 \rightarrow AFF$, the slopes are negative but with a magnitude larger than S_0/μ. Moreover, for the transition line between AFP and AFF phase, the model gives a slope $S_0/\mu = 5$ kOe/K, in good agreement with these of the transition line corresponding to an increase of K_z domain. Thus this transition line may be considered as the boundary between AFF and AFP phases, in addition this line intersects the temperature axis at $T\simeq7$ K, temperature which corresponds to the AFF → AFP transition determined by magnetic measurements.

Nevertheless, the slope of the transition line between FP phases and the paramagnetic state has a value (16 ± 2 kOe/K) three times larger than S_0/μ. This difference can be explained if we assume that the entropy of nonmagnetized planes is not the same in the FP phase (S_0) and the paramagnetic state (S_0'). If the FP phase is characterized by a propagation vector $\vec{k}$, the calculated slope is given by

$$H/T = S_0/\mu + (S_0' - S_0)/\mu(1-k)\,.$$

So using $S_0/\mu = 5$ kOe/K ($S_0 = k\ln2$) and $k=\frac{6}{11}$ we deduce $S_0'/\mu = 10$ kOe/K, i.e., $S_0'/k = 1.4\pm0.2 \simeq \ln4$. This result suggests that the crystal-field level splitting is quite different for a Ce^{3+} ion in the paramagnetic state and in P planes for FP or AFP phases. In the paramagnetic state, the value of the entropy (~1.4 at 18 K) indicates that the ground state is the doublet Γ_7, this value is consistent with the $\Gamma_7 - \Gamma_8$ splitting (38 K at 20 K) given by

TABLE IV. Comparison between experimental and calculated slopes of phase boundary lines.

Change of phase I → II	Phase I	Phase II	Calc.	Slope (dH/dT) Expt. (kOe/K)	Slope (dH/dT) Calculated from $S_0 = k\ln2$ (kOe/K)
FP → FP	FP_1 FP_2 FP_3 FP_4	FP_2 FP_3 FP_4 F	S_0/μ	6 ± 1	4.9
FP → AFF	FP_3	S' ($k=\frac{2}{3}$)	$-2S_0/\mu$	-11.5 ± 1	−9.8
	FP_4	S' ($k=\frac{2}{3}$)	$-\frac{3}{2}S_0/\mu$	-6 ± 2	−7.3
FP → AFP	FP_2	S_2 ($k=\frac{4}{7}$)	$-\frac{5}{7}S_0/\mu$	-3.5 ± 1	−3.5
	FP_3	S_2 ($k=\frac{4}{7}$)	$-\frac{31}{35}S_0/\mu$	-5 ± 1	−4.4
AFP → AFF	S_2 (high T)	S_2 (low T)	S_0/μ	5 ± 1	4.9
FP → P	FP_1	P	S_0/μ	16	See text
AFF → AFF	S_2	S'	0	0	
	S'	F	0	0	

Heer.[32] This level scheme is the same as for diluted compounds[27] and gives an easy magnetization axis along [111]. This result is in contrast with the strong anisotropy along a fourfold axis observed below T_N. To take into account for this fact Cooper *et al.*[27] have proposed strong anisotropic interactions. But an alternative proposal is to consider that the tetragonal distortion may induce a modification of the crystal-field levels in order to give a ground-state doublet allowing a large moment value and a strong anisotropy along the tetragonal axis. This doublet may be quite different from the Γ_7 doublet which is considered by Wang *et al.*[11] to interpret the susceptibility anomaly below T_N. In fact in very low field no anomaly has been observed by Hulliger *et al.*[18] The phase diagram (Fig. 3) indicates that an abnormal behavior of the susceptibility occurs in field higher than 4 kOe, where FP phases appear; this value may depend on the crystal quality.

The susceptibility and specific-heat anomalies[18] near $\frac{1}{2}T_N$ are well explained by a AFP → AFF phase transition. Considering only bilinear exchange interactions this temperature (7–8 K) corresponds to the exchange energy of a ferromagnetic (001) plane.

The existence of a weak crystal-field splitting allows higher-order interaction terms. Cooper *et al.*[27] have proposed an anisotropic exchange interactions of the form $J_{iz}J_{jz}^3$ to explain the magnetic behavior of CeBi which exhibits a phase transition at $\frac{1}{2}T_N$ between a phase $k=1(+--+-)$ and a phase $k=\frac{1}{2}(++--++--)$. On the other hand Levy *et al.*[44] suggest that anisotropic interactions would be rather biquadratic $J_{iz}^2 J_{jz}^2$ reflecting quadrupolar interactions. However, it is also possible to explain the existence of an AFP or FP order by bilinear interactions assuming an Ising model.

Nevertheless, whatever the nature of the interactions they must be of very long range in the direction of the tetragonal axis to account for the large and numerous magnetic cells which have been observed. In these conditions, it is most likely that, in addition to isotropic or anisotropic exchange interactions, long range interactions via phonons may exist. This type of interaction implies a strong spin-lattice coupling which mixes the magnetic order with a Jahn-Teller effect. This coupling has been proposed in UO_2.[45,46] It must be noted that uranium compounds[47] exhibit a magnetic behavior similar to CeSb and CeBi.

CONCLUSION

Neutron-diffraction experiments have provided very new and important results about the magnetic structures and the phase diagram of the quite complicated rare-earth compound CeSb. The unusual phase diagram has been justified by simple thermodynamic considerations. The most important result is the observation of magnetic structures consisting of ordered sequences of ferromagnetic and "paramagnetic" planes. From these results it is possible to describe in an homogenous way the magnetic behavior of CeSb. Nevertheless, they rise some theoretical questions, in particular the nature of the so-called paramagnetic planes in the ordered state.

To explain this unusual order it is necessary to introduce long-range interactions which may be due to a strong spin-lattice coupling. More extensive experimental investigations must be done in order to give a definitive answer to this question. In particular, magnetic anisotropy studies, a phase-diagram determination for an applied field along a [111] direction, and a dynamical study of the spin-lattice coupling would provide fruitful informations. We hope that these results will stimulate theoretical developments.

ACKNOWLEDGMENTS

We thank I. S. Jacob and B. R. Cooper for stimulating our interest in this subject.

APPENDIX

This appendix deals with the neutron scattering by magnetic structures consisting of a periodic stacking of (001) planes for a fcc lattice. In a plane, the moments are assumed to be ferromagnetically aligned along a direction perpendicular to the plane (along z). The magnitude μ of a Ce^{3+} magnetic moment changes from plane to plane according to a periodic function $f(z)$ characterized by a wave vector $\vec{q}=(0,0,q)$ with $q=2\pi/Z$ [$q=(2\pi/a)k$]. This periodic function can be expanded in Fourier series

$$f(z)=\sum_{m=-\infty}^{\infty} a_m e^{imqz}. \tag{A1}$$

Equation (A1) does not represent the Fourier components of the magnetic moment because the distribution is not continuous. For a magnetic moment distribution $\vec{\mu}_i=(0,0,\mu(z_i))$ the Fourier components $\mu_{q'}$ of $\mu(z_i)$ can be deduced from (A1).

$$\mu_{q'}=\sum_{m=-\infty}^{+\infty} A_m \delta(mq-q'-L). \tag{A2}$$

Equation (A2) means that neutron diffraction will occur only for scattering vectors $\vec{H}_N+\vec{q}'$ [$\vec{H}_N$ is a reciprocal-lattice vector (h,k,l)], with $\vec{q}'\equiv(0,0,q')$ such as

$$q'=mq-L. \tag{A3}$$

For each value of m, L is defined in order to get

the wave vector $\vec{q}'$ in the first Brillouin zone. For a fcc lattice L is given by $L = 2l2\pi/a$ and q' is limited to $-2\pi/a < q' < 2\pi/a$. So the fundamental Fourier component corresponds to $q' = q$, the second-order harmonic to $q' = 2q - L$, etc. But two vectors $\vec{q}'$ will be equivalent if $\vec{q}_1' - \vec{q}_2'$ is a reciprocal vector, i.e., $(m_1 - m_2)q = L$. This condition cannot be satisfied if q is incommensurate with the lattice, thus all q' are different and $\mu_{q'}$ is given by the Fourier expansion of $f(z)$:

$$\mu_{q'=mq-L} = a_m .$$

Whereas if q is commensurate with the lattice $q = (2\pi/a)n_1/n_2$ (n_1 and n_2 are integer numbers), q' will take a finite number of values because $m_1 - m_2 = 2ln_2/n_1$. If n_1 is odd, there are $2n_2$ values; whereas if n_1 is even, only n_2 values exist. The Fourier components $\mu_{q'}$ are given by (A2), where the summation must be done only for $m = p + nl$,

$$\mu_{q_p'} = \sum_{l=-\infty}^{+\infty} a_{p+nl} , \tag{A4}$$

where $n = 2n_2$ or n_2 according to the parity of n_1 and $p = 1, 2, 3, \ldots, n$.

To go further we consider the function $f(z)$ defined by

$$f(z) = \begin{cases} -B & \text{if } 0 < z < z_0 , \\ 0 & \text{if } z = z_0 , \\ A & \text{if } z_0 < z < z_0 + z_1 , \\ 0 & \text{if } z = z_0 + z_1 , \\ -B & \text{if } z_0 + z_1 < z < Z = 2\pi/q . \end{cases} \tag{A5}$$

For such a function a_m is given by

$$\begin{aligned} a_m &= (i/2\pi m)(A+B)e^{im\phi_0}(e^{im\phi_1} - 1) , \\ a_0 &= (1/2\pi)[A\phi_1 - B(2\pi - \phi_1)] , \end{aligned} \tag{A6}$$

with

$$\phi_0 = qz_0 \text{ and } \phi_1 = qz_1 .$$

Equation (A6) shows that $a_{2m} = 0$ if $\phi_1 = \pi$, i.e., if $f(z)$ is a square-wave function. Therefore, if n is even ($n = 2n_2$ for n_1 odd), only Fourier components $\mu_{q_p'}$ associated to odd p values exist because in (A4) all terms have the same parity. Whereas if $n = n_2$ is odd (n_1 = even), p can take an odd or even value and all the harmonics exist. By writing (A4) as

$$\mu_{q_p'} = \sum_{l=-\infty}^{+\infty} a_{p+2n_2 l} + \sum_{l=-\infty}^{+\infty} a_{p+n_2+2n_2 l} , \tag{A7}$$

for p odd

$$\mu_{q_p'} = \sum_{l=-\infty}^{+\infty} a_{p+2n_2 l} , \tag{A8}$$

and for p even

$$\mu_{q_p'} = \sum_{l=-\infty}^{+\infty} a_{p+n_2+2n_2 l} . \tag{A9}$$

Equation (A9) is equivalent to (A8) if p is replaced by $p' = p + n_2$; therefore p' can take only odd values between 1 and $2n$ as for the first case. So for a square-wave function only the Fourier components associated to odd p values between 1 and $n = 2n_2$ must be taken into account. Whereas for a non-square-wave function the Fourier components corresponding to even p values can have a large amplitude because the coefficients a_{2p} are different from zero.

As in CeSb the strongest harmonics corresponds to $p = 1$ and 3 we can conclude that the structures are square-wave ones.

So the calculation of the harmonic amplitudes will be limited to only square-wave functions. Within this condition (A4) becomes

$$\mu_{q_p'} = \frac{i}{\pi}(A+B)\sum_{l=-\infty}^{+\infty} \frac{e^{i(p+2n_2 l)\phi_0}}{p + 2n_2 l} , \tag{A10}$$

with $p = 1, 3, 5, \ldots, 2n_2 - 1$ (n_2 values). ϕ_0 represents the phase of $f(z)$ in respect to the lattice [the (001) planes are located at $z = 0, \frac{1}{2}a, a, \ldots, r\frac{1}{2}a, \ldots$] and can take any value between 0 and 2π.

In (A10) the sum $S_P(\phi_0)$ can be evaluated by considering the periodic function defined, in the range $-\pi/n < \phi' < \pi/n$, by

$$F(\phi') = e^{-ip\phi'} , \tag{A11}$$

with a period $2\pi/n$. Such a function can be expanded in Fourier series

$$e^{-ip\phi'} = \sum_{l=-\infty}^{+\infty} (-1)^l \frac{n}{\pi} \frac{\sin p\pi/n}{p + nl} e^{-inl\phi'} . \tag{A12}$$

By defining

$$\phi = \phi' + (\pi/n)(2j+1) , \tag{A13}$$

(A12) gives

$$S_P(\phi) = \frac{\pi}{n \sin} \sin p\pi/n e^{ip(\pi/n)(2j+1)} . \tag{A14}$$

Equation (A14) is valid only for $2j\pi/n < \phi < 2(J+1)\pi/n$. If j takes the value $0, 1, \ldots, n-1$, ϕ runs from 0 to 2π except the values $\phi = 2j\pi/n$. Therefore

$$\mu_{q_p'} = \frac{i(A+B)}{2n_2 \sin p\pi/2n_2} e^{ip(\pi/2n_2)(2j+1)} , \tag{A15}$$

if

$$\phi_0 \neq 2j\pi/2n_2 . \tag{A16}$$

Equation (A15) shows that the amplitude of the harmonic p does not depend on ϕ_0 since only the phase is ϕ_0 dependent. If $\phi_0 = 2j\pi/2n_2$, (A10) becomes

$$\mu_{q_p'} = \frac{i(A+B)}{\pi} e^{ipj\pi/n_2} \sum_{l=-\infty}^{+\infty} \frac{1}{p + 2n_2 l} . \tag{A17}$$

It can be shown that

$$\sum_{l=-\infty}^{+\infty} \frac{1}{p+2n_2 l} = \frac{\pi}{2n_2} \cot \frac{p\pi}{2n_2} .$$

Thus

$$\mu_{q'_p} = \frac{i(A+B)}{2n_2 \tan p\pi/2n_2} e^{ipj\pi/n_2} , \quad \text{(A18)}$$

if $\phi_0 = 2j\pi/2n_2$. Equation (A18) indicates also that the amplitude of $\mu_{q'_p}$ is independent of ϕ_0. Thus the Fourier components $\mu_{q'_p}$ can take only two values according to ϕ_0 is equal or not to $2j\pi/2n_2$. We shall see now what means that

$$\phi_0 = 2j\pi/2n_2 . \quad \text{(A19)}$$

Using (A6), (A19) gives

$$z_0 = \tfrac{1}{2} a j/n_1 , \quad \text{(A20)}$$

with $j = 0, 1, 2, \ldots, 2n_2 - 1$. By definition $f(z) = 0$ if $z = z_0 + \lambda \frac{1}{2} Z$, i.e.,

$$z = \tfrac{1}{2} a(j + \lambda n_2)/n_1 , \quad \text{(A21)}$$

with $\lambda = 0, 1, \ldots, 2n_1 - 1$. If r labels the $2n_2$ (001) planes of a magnetic cell, (A21) means that some planes will be nonmagnetic if

$$z_r = r\tfrac{1}{2}a = \tfrac{1}{2} a(j + \lambda n_2)/n_1 . \quad \text{(A22)}$$

So for a j value (A22) gives the labels of the planes which are paramagnetic; it can be seen easily that such planes exist every n_2 planes. For example, if $j = 0$, the planes $r = 0, n_2, 2n_2$, etc., are paramagnetics. Therefore the choice of j corresponds to select two paramagnetics planes in the magnetic cell, and (A18) shows that this choice gives a phase shift for $\mu_{q'}$. We shall summarize now the results by considering the magnetic structures observed for CeSb.

The amplitude of a Fourier component $\mu_{q'_p}$ determined by neutron experiments is defined as

$$\mu_{q'_p} = \tfrac{1}{2} A_{q'_p} e^{i\psi_{q'_p}} \quad \text{if } \vec{q}'_p \neq \tfrac{1}{2}\vec{H}_N \quad \text{(A23)}$$

and

$$\mu_{q'_p} = A_{q'_p} \quad \text{if } \vec{q}'_p = \tfrac{1}{2}\vec{H}_N .$$

In the text the reduced wave vector $\vec{k}'$ is used instead of: $\vec{q}' = (2\pi/a)\vec{k}'$.

A. Magnetic structures of type AFF

In this case all the planes are magnetic, thus $\phi_0 \neq 2j\pi/2n_2$ and $A = B = \mu_{Ce}$:

$$\mu_{q'_p} = \frac{i\mu_{Ce}}{n_2 \sin p\pi/2n_2} e^{ip(\pi/2n_2)(2j+1)} . \quad \text{(A24)}$$

If $\vec{q}'_p \neq \frac{1}{2}\vec{H}_N$,

$$A_{q'_p} = \frac{2\mu_{Ce}}{n_2 \sin p\pi/2n_2} . \quad \text{(A25)}$$

From (A25) the value of the harmonics can be calculated. In particular, for the fundamental term ($q'_1 = q$) (A25) gives

$$A_q = \frac{2\mu_{Ce}}{n_2 \sin \pi/2n_2} . \quad \text{(A26)}$$

Thus for $n_2 = 2 \rightarrow A_q = \sqrt{2}\,\mu_{Ce}$,

$n_2 = 3 \rightarrow A_q = \frac{4}{3}\mu_{Ce}$.

For large values of n_2, $\sin\pi/2n_2 \# \pi/2n_2$, and $A_q \# (4/\pi)\mu_{Ce}$, i.e., (A26) gives the values which correspond to the Fourier expansion of a continuous function. In this case the amplitude of the harmonics decreases as $1/P$, whereas in fact it decreases only as $(\sin p\pi/2n_2)^{-1}$.

The harmonics associated to $\vec{q}'_p = \frac{1}{2}\vec{H}_N$, i.e., $q' = 0$ or $2\pi/a$ ($k' = 0$ or 1), correspond to $p = n_2$, and then exist only if n_2 is odd. Two cases must be considered: (i)n_1 = odd: Only the component $k = 1$ exists and $A_{k=1} = \mu_{Ce}/n_2$. (ii)n_1 = even: Only the component $k = 0$ exists and $A_{k=0} = \mu_{Ce}/n_2$. Thus a ferromagnetic component μ_{Ce}/n_2 can exist only if n_1 is even. If n_1 is odd, the structure is antiferromagnetic.

B. Magnetic structures of type AFP

They correspond to $A = B = \mu_{Ce}$ and $\phi_0 = 2j\pi/2n_2$. So

$$A_{q'_p} = \frac{2\mu_{Ce}}{n_2 \tan p\pi/2n_2} \quad \text{(A27)}$$

and $A_{q'=0,1} = 0$. For example, if $n_2 = 3$ ($k = \frac{2}{3}$), the presence of paramagnetic planes reduces the amplitude of the fundamental term from $\frac{4}{3}\mu_{Ce}$ to $(2/\sqrt{3})\mu_{Ce}$.

C. Magnetic structures of type FP

These structures can be obtained by doing $A = \mu_{Ce}$, $B = 0$, and $\phi_0 \neq 2j\pi/2n_2$, thus

$$A_{q'_p} = \frac{\mu_{Ce}}{n_2 \sin p\pi/2n_2} . \quad \text{(A28)}$$

In this case it exists always a component $q' = 0$ with an amplitude which is given by adding the contribution of the harmonic $p = n_2$ and a term $\frac{1}{2}\mu_{Ce}$ which represents the mean value

$$A_{q'=0} = \tfrac{1}{2}\mu_{Ce}(1 + 1/n_2)$$

thus

$$\mu_{ferro} = \mu_{Ce}(n_2 + 1)/2n_2 . \quad \text{(A29)}$$

In Table V are reported the numerical values of the harmonic amplitudes corresponding to the various square-wave structures which have been ob-

TABLE V. Amplitudes of the harmonics for AFF, AFP, and FP phases.

$k=n_1/n_2$			$p=1$	3	5	7	9	11	13	15	17	19	21
	k'		$\frac{2}{3}$	0	$-\frac{2}{3}$								
$k=\frac{2}{3}$	$A_{k'}/\mu_{Ce}$	AFF	$\frac{4}{3}$	$\frac{1}{3}$	$\frac{4}{3}$								
		AFP	$2/\sqrt{3}$	0	$2/\sqrt{3}$								
	k'		$\frac{4}{7}$	$-\frac{2}{7}$	$\frac{6}{7}$	0	$-\frac{6}{7}$	$\frac{2}{7}$	$-\frac{4}{7}$				
$k=\frac{4}{7}$	$A_{k'}/\mu_{Ce}$	AFF	1.284	0.458	0.317	$\frac{1}{7}$	0.317	0.458	1.284				
		AFP	1.252	0.358	0.137	0	0.137	0.358	1.252				
	k'		$\frac{5}{9}$	$-\frac{3}{9}$	$\frac{7}{9}$	$-\frac{1}{9}$	1	$\frac{1}{9}$	$-\frac{7}{9}$	$\frac{3}{9}$	$-\frac{5}{9}$		
$k=\frac{5}{9}$	$A_{k'}/\mu_{Ce}$	AFF	1.280	0.444	0.290	0.236	$\frac{1}{9}$	0.236	0.290	0.444	1.280		
		AFP	1.260	0.385	0.186	0.081	0	0.081	0.186	0.385	1.260		
$k=\frac{1}{2}$	k'	AFF	$\frac{1}{2}$	$-\frac{1}{2}$									
	$A_{k'}/\mu_{Ce}$		$\sqrt{2}$	$\sqrt{2}$									
FP	k'		$\frac{2}{5}$	$-\frac{4}{5}$	0	$\frac{4}{5}$	$-\frac{2}{5}$						
$k=\frac{2}{5}$	$A_{k'}/\frac{1}{2}\mu_{Ce}$		1.294	0.494	$\frac{1}{5}$	0.494	1.294						
FP	k'		$\frac{4}{9}$	$-\frac{6}{9}$	$\frac{2}{9}$	$-\frac{8}{9}$	0	$\frac{8}{9}$	$-\frac{2}{9}$	$\frac{6}{9}$	$-\frac{4}{9}$		
$k=\frac{4}{9}$	$A_{k'}/\frac{1}{2}\mu_{Ce}$		1.280	0.444	0.290	0.236	$\frac{1}{9}$	0.236	0.290	0.444	1.280		
FP	k'		$\frac{6}{11}$	$-\frac{4}{11}$	$\frac{8}{11}$	$-\frac{2}{11}$	$\frac{10}{11}$	0	$-\frac{10}{11}$	$\frac{2}{11}$	$\frac{8}{11}$	$\frac{4}{11}$	$-\frac{6}{11}$
$k=\frac{6}{11}$	$A_{k'}/\frac{1}{2}\mu_{Ce}$		1.277	0.437	0.277	0.216	0.189	$\frac{1}{11}$	0.189	0.216	0.277	0.437	1.277

served for CeSb. In the case of a non-square-wave structure the same procedure can be done by using (A6). For example, the structure $+++-$, observed for CeBi, corresponds to $k=\frac{1}{2}$. Thus all the harmonics are present: $p=1\rightarrow k=\frac{1}{2}$, $p=2\rightarrow k=1$, $p=3\rightarrow k=-\frac{1}{2}$, and $p=4\rightarrow k=0$. Whereas for a square-wave structure with $k=\frac{1}{2}$ only the harmonics $p=1(k'=\frac{1}{2})$ and $p=3(k'=-\frac{1}{2})$ exist.

*Present address: Institute of Physics, A. S. C. Peking, China.

[1]A. Iandelli, Z. Anorg. Allg. Chem. 288, 81 (1956).
[2]K. A. Gschneidner, Rare Earth Alloys (Van Nostrand, Princeton, 1961), p. 375.
[3]G. Busch, P. Junod, F. Levy, A. Menth, and O. Vogt, Phys. Lett. 14, 264 (1965).
[4]T. Tsuchida and W. E. Wallace, J. Chem. Phys. 43, 2087 (1965); 43, 2885 (1965).
[5]G. Busch and O. Vogt, Phys. Lett. 20, 152 (1966).
[6]T. Tsuchida and Y. Nakamura, J. Phys. Soc. Jpn. 25, 284 (1968).
[7]B. Rainford, K. C. Turberfield, G. Busch, and O. Vogt, J. Phys. C 1, 679 (1968).
[8]G. Meier and O. Vogt, AF-SSP-87, 8 (1975) (unpublished).
[9]E. D. Jones, Phys. Lett. 22, 266 (1966).
[10]E. D. Jones, Phys. Rev. 180, 455 (1969).
[11]Y. L. Wang and B. R. Cooper, Phys. Rev. B 2, 2607 (1970).
[12]G. Busch and O. Vogt, Phys. Lett. A 25, 449 (1967).
[13]T. Tsuchida and Y. Nakamura, J. Phys. Soc. Jpn. 22, 942 (1967).
[14]H. Bartholin, I. S. Jacobs, B. R. Cooper, and O. Vogt, Bull. Am. Phys. Soc. 17, 248 (1972).
[15]B. R. Cooper, M. Landolt, and O. Vogt, *International Conference on Magnetism, Moscow, 1973* (Nauka, Moscow, 1974).
[16]T. Tsuchida, A. Hashimoto, and Y. Nakamura, J. Phys. Soc. Jpn. 36, 685 (1974).
[17]H. Bartholin, D. Florence, Wang Tcheng-Si, and O. Vogt, CiBi: Phys. Status Solidi A 24, 631 (1974); CeSb: 29, 275 (1975).
[18]F. Hulliger, M. Landolt, H. R. Ott, and R. Schmelczer, J. Low Temp. Phys. 20, 269 (1975).
[19]N. Nereson and G. Arnold, J. Appl. Phys. 42, 1625 (1971).
[20]T. Tsuchida, T. Suzawa, and Y. Nakamura, Phys. Status Solidi B 44, K25 (1971).
[21]J. W. Cable and W. C. Koehler, AIP Conf. Proc. 5, 1381 (1972).
[22]G. H. Lander, M. H. Mueller, and O. Vogt, AIP Conf. Proc. (1975) (to be published).
[23]B. Lebech, P. Fischer, and B. D. Rainford, Rare Earth and Actinides, Durham, 1971, Vol. 3, p. 204 (unpublished).

[24]P. Fischer, G. Meier, and O. Vogt, Eidgenössische Institut für Reaktotechnik, AF.SSP-84 Würenlingen (1975) (unpublished).
[25]F. Levy, Phys. Kondens. Mater. 10, 85 (1969).
[26]G. Busch, W. Stutius, and O. Vogt, J. Appl. Phys. 42, 1493 (1971).
[27]B. R. Cooper and O. Vogt, J. Phys. C 32, 1026 (1971).
[28]B. R. Cooper, A. Furrer, W. Buhrer, and O. Vogt, Solid State Commun. 11, 21 (1972).
[29]A. Furrer, W. Bührer, H. Heer, W. Hälg, J. Benes, and O. Vogt, *Neutron Inelastic Scattering Conference* (I.A.E.A., Grenoble, 1972), p. 563.
[30]R. J. Birgeneau, E. Bucher, J. P. Maita, L. Passell and K. C. Turberfield, Phys. Rev. B 8, 5345 (1973).
[31]G. Meier and O. Vogt, AF-SSP 93, 9 (1975) (unpublished).
[32]H. Heer, Eidgenössische Institut für Reaktotechnik, AF. SSP. 84, Würenlingen (1975) (unpublished).
[33]G. Meier and O. Vogt, AF-SSP-87, 8 (1975) (unpublished).
[34]S. M. Myers and A. Narath, Solid State Commun. 12, 83 (1973); Phys. Rev. B 9, 227 (1974).
[35]T. Tsuchida, S. Onga, T. Kawai, and S. Kawarazaki, J. Phys. Soc. Jpn. 35, 1788 (1973).
[36]P. Schobinger, P. Fischer and O. Vogt, Eidgenossische Institut für Reaktotechnik, AF-SSP-57, Würenlingen (1972) (unpublished).
[37]H. Heer, A. Furrer, and O. Vogt, Eidgenössische Institut für Reaktotechnik, AF. SSP. 74, Würenlingen (1974) (unpublished).
[38]A. Furrer, W. Halg, and T. Schneider, *Neutron Inelastic Scattering* (I.A.E.A., Vienna, 1968), Vol. II, p. 133.
[39]K. W. H. Stevens and E. Pytte, Solid State Commun. 13, 101 (1973).
[40]G. Aubert, H. Bartholin, D. Bloch, J. Chaussy, M. Guillot, A. Lacaze, J. Paueau, R. Pauthenet, J. C. Picoche, P. Rub, J. C. Vallier, and A. Waintal, *International Conference on Magnetism, Moscow, 1973* (Nauka, Moscow, 1974).
[41]J. Rossat-Mignod, thesis (University of Grenoble, 1972) (unpublished).
[42]MIT report (1972) (unpublished).
[43]M. Blume, A. J. Freeman, and R. E. Watson, J. Chem. Phys. 37, 1245 (1962).
[44]M. Levy and H. H. Chen, AIP Conf. Proc. No. 5, 373 (1972).
[45]R. A. Cowley and G. Dolling, Phys. Rev. 167, 464 (1969).
[46]S. J. Allen, Phys. Rev. 167, 492 (1968).
[47]G. H. Lander and M.H. Mueller, Phys. Rev. B 10, 1994 (1974).